Electronic Supplementary Information

Solid-state reactivity for simple, environmentally-friendly separation of scandium and synthesis of new metal-organic materials

Igor Huskić, Mihails Arhangelskis and Tomislav Friščić

Contents

1. Methods and Materials

Chemicals used in the experiments were used as obtained, except in the case of Gd_2O_3, Nd_2O_3, La_2O_3 and Eu_2O_3 which were calcined at 800 ºC for 24 hours to ensure the conversion of potential hydroxide species to oxide. Oxalic acid (H_2**ox**), potassium oxalate (K_2**ox**), sodium oxalate (Na_2**ox**) and ammonium oxalate ($(NH_4)_2$**ox**) were obtained from Sigma Aldrich. Homogenization of the mixtures was achieved by 30 seconds milling in a Retsch MM400 shaker mill, using a single 10 mm diameter zirconia ball (weight of ca. 3.6 grams) for solid reaction mixtures that were all of ca. 200 mg size. Relative humidity was controlled via a saturated solution of potassium sulfate[1] ensuring that the humidity never exceeded 98%, and was kept within 96%±0.5% for reactions at 45 ºC.

Powder X-ray Diffraction (PXRD) data was collected on a PROTOXRD AXRD benchtop instrument equipped with a DECTRIS MYTHEN2R 1D detector, using nickel-filtered CuK_α (λ = 1.5418 Å) radiation. Conversion of file formats was performed in the PowDLL program suite.[2]

Crystal Structures of Na_3Sc**ox**$_3\cdot 6H_2O$ (**4**), K_3Sc**ox**$_3\cdot 4H_2O$ (**5**), K_8Sc_2**ox**$_7\cdot 10H_2O$ (**6**) and K_3Gd**ox**$_3\cdot 3H_2O$ (**7**) were determined by single crystal X-ray diffraction, using a Bruker D8 ADVANCE X-ray diffractometer equipped with a PHOTON100 detector and graphite-monochromated Mo$K\alpha$ (λ = 0.71073 Å) radiation. The X-ray diffraction data sets were collected using the ω- and φ- scan mode over a 2θ-range up to 54º. The structures were solved by intrinsic phasing implemented in SHELXT[3] and refined using SHELXL.[4] Structure refinement was performed on F^2 using all data. Hydrogen atoms participating in hydrogen bonds were located from the electron density map whenever data quality was sufficient. Otherwise, they were fixed to appropriate distances and refined from the electron density map.

Crystal structures of Lu_2**ox**$_3\cdot 6H_2O$ (**1**), $(NH_4)Sc$**ox**$_2\cdot 2H_2O$ (**2**), $(NH_4)Yb$**ox**$_2\cdot H_2O$ (**3**) and K_3Eu**ox**$_3\cdot 3H_2O$ (**8**) were solved from powder X-ray data that were collected on a Bruker D8 Venture instrument equipped with a CuKα non-monochromated X-ray source. The measurements were performed under Bragg-Brentano geometry, with the sample material placed on a spinning plate. The unit cell determination was achieved using DICVOL06[5] algorithm, accessed via graphical interface of the program DASH.[6] The unit cell parameters were then refined using the Pawley procedure[7] and the extracted diffraction intensities were used for space group determination. Simulated annealing (SA) structure solution and Rietveld refinement were then performed in the program TOPAS Academic v.6.[8] Diffraction peak shapes were modelled with a pseudo-Voigt function, while the background was described with 8th order Chebyshev polynomial function. During the SA structure solution peak shape, background terms and the unit cell parameters were kept fixed, while the metal and water oxygen atoms were allowed free movement. In addition, the geometry of the **ox** fragments was defined using rigid body approach, with their positions and orientations freely refined during SA calculation. The structural model with the lowest R_{wp} value was selected for Rietveld refinement.[9] At this point all the previously fixed parameters (background, peak shape and zero shift) were freely refined. In addition, atomic thermal motion was modelled with a single isotropic Debye-Waller factor.

Structures have been deposited with the Cambridge Structural Database, deposition codes 1963550-1963557.

Fourier-transform infrared attenuated total reflectance (FTIR-ATR) measurements were performed on a Bruker VERTEX 70 instrument equipped with a PLATINUM diamond crystal ATR unit.

Thermogravimetric and differential scanning calorimetry (TGA and DSC) analysis was performed on a Mettler-Toledo TGA DSC 1 Star system thermobalance using alumina crucibles under an stream of nitrogen (50 ml min^{-1}) and a heating rate of 5 °C min^{-1} from 25 °C until 200 °C and in a stream of air (50 ml min^{-1}) and a heating rate of 10 °C min^{-1} from 200 °C to 700 °C Sample size was between 2 mg and 10 mg. Results were processed with the Mettler STARe 9.01 software.

Elemental analysis was performed by Thermo Fisher Scientific iCAPQc ICP-MS equipped with a CETAC ASX520 autosampler.

Mixture of rare earths were reacted with oxalic acid and sodium or ammonium oxalate in a 1:3:3 stoichiometric ratio. After 10 days of aging at 90 ºC and ~90% relative humidity, a 200 mg sample of the mixture was suspended in distilled water and heated to boil. The liquid, mostly containing dissolved Sc species, was filtered and the solid residue was digested with 4% analytical grade nitric acid. All samples were diluted to concentrations between 50 ppb and 1 ppm appropriate for ICP-MS.

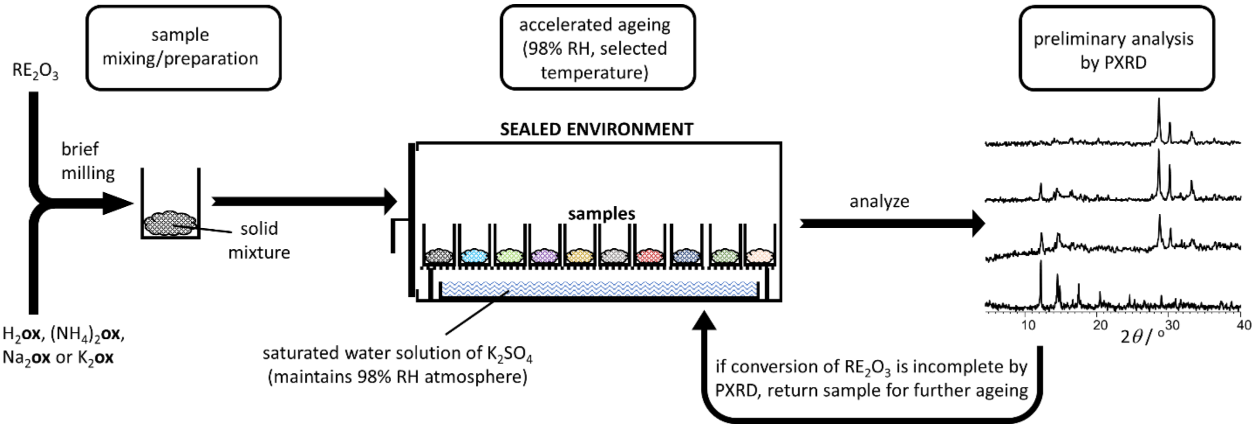

Figure S1. Schematic illustrating the sample preparation and the accelerated ageing procedure used in this work.

2. Results of Rietveld refinement

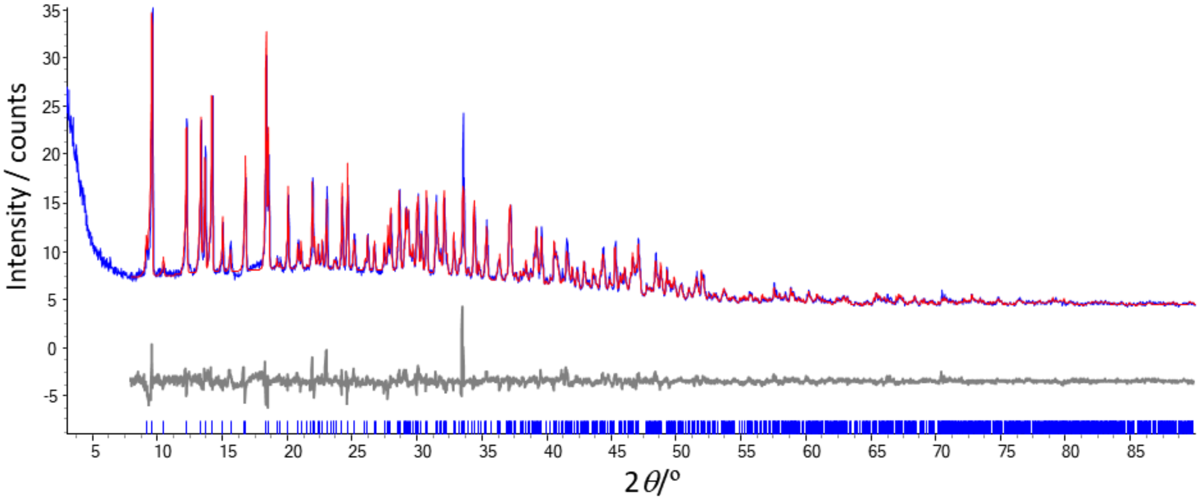

Figure S2. Final Rietveld fits for structure solution using X-ray powder data for $K_3Eu\mathbf{ox}_2\cdot 3H_2O$ (**8**). Measured pattern is shown in blue, simulated in red and the residual is shown in grey. Vertical blue lines denote positions of expected reflections. Pattern quality is somewhat poor due to X-ray fluorescence of Eu(III) under Cu *K*$_\alpha$ wavelength.

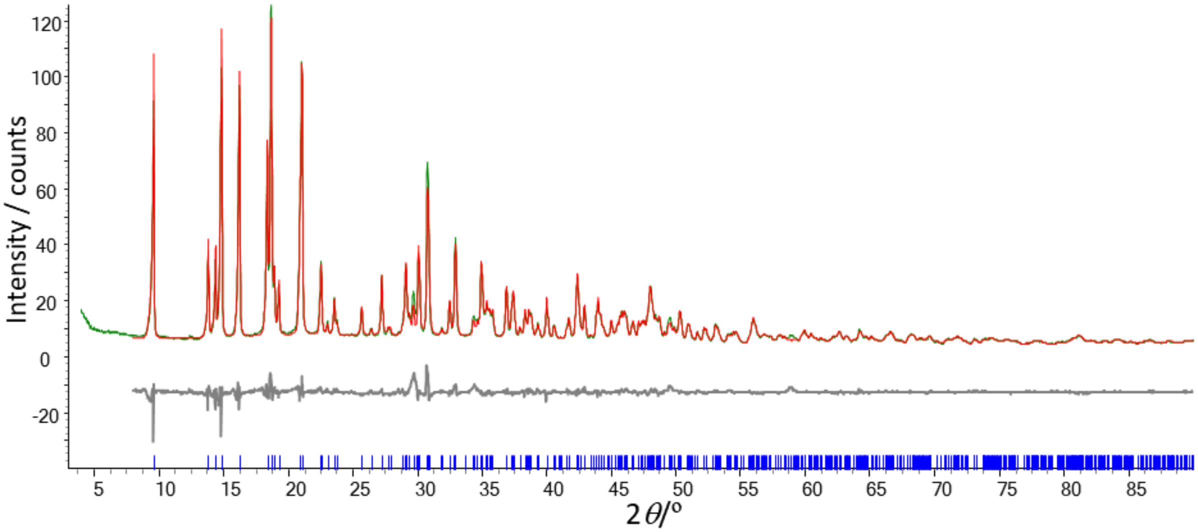

Figure S3. Final Rietveld fits for structure solution using X-ray powder data for $Lu_2\mathbf{ox}_3\cdot6H_2O$ (**1**). Measured pattern is shown in green, simulated in red and the residual is shown in grey. Vertical blue lines denote positions of expected reflections.

3. Crystallographic Information

Table S1. Crystallographic parameters of the structures determined by single crystal diffraction data in this work.

Compound	$Na_3Sc\mathbf{ox}_3\cdot 6H_2O$ (**4**)	$K_8Sc_2\mathbf{ox}_7\cdot 10H_2O$ (**6**)	$K_3Sc\mathbf{ox}_3\cdot 4H_2O$ (**5**)	$K_3Gd\mathbf{ox}_3\cdot 3H_2O$ (**7**)
M_r	484.07	599.51	498.38	592.66
Crystal system	Monoclinic	Monoclinic	Monoclinic	Triclinic
Space group	$I2/a$	$C2/c$	$C2/c$	$P–1$
a / Å	17.851(2)	15.8839(14)	11.4151(8)	8.4795(8)
b / Å	11.0413(7)	11.4558(10)	12.6781(9)	9.3708(9)
c / Å	18.2806(13)	22.7314(19)	11.4093(8)	9.7323(9)
α / °	90	90	90	98.377(4)
β / °	104.189(2)	92.190(4)	111.900(2)	91.097(4)
γ / °	90	90	90	96.629(4)
V / Å^3	3493.1(5)	4133.2(6)	1532.02(19)	759.45(12)
Z	8	8	4	2
ρ_{calc} / g cm^{-3}	1.841	1.927	2.161	2.592
Refln. measured	44915	35859	19621	45874
Unique refln.	8442	4080	1741	5886
T / K	100	273	100	100
R_1 (%)	3.73	5.04	1.80	1.74
wR_2 (%)	8.29	6.29	4.74	3.69
S	1.032	1.049	1.102	1.046

Table S2. Crystallographic parameters of structures determined from powder diffraction data in this work.

Compound	Lu_2**ox**$_3$·$6H_2O$ (**1**)	NH_4Sc**ox**$_2$·$2H_2O$ (**2**)	NH_4Yb**ox**$_2$·H_2O (**3**)	K_3Eu**ox**$_3$·$3H_2O$ (**8**)
Crystal system	Triclinic	Hexagonal	Monoclinic	Triclinic
Space group	P–1	$P6_222$[a]	$P2/n$	P–1
a / Å	9.5867(2)	9.0093(2)	9.0427(2)	8.4883(2)
b / Å	6.64358(16)	9.0093(2)	6.09117(12)	9.3894(3)
c / Å	6.25859(16)	11.2503(4)	7.8999(2)	9.7552(2)
α / °	98.1966(17)	90	90	98.255(2)
β / °	99.4509(19)	90	90.182(3)	91.154(2)
γ / °	75.113(2)	120	90	96.544(3)
V / Å^3	377.9	790.9	435.1	763.9
Z	2	3	2	2
ρ_{calc} / g cm^{-3}	3.120	1.682	2.893	2.527
R_p / %	1.1	5.1	3.1	3.3
R_{wp} / %	5.2	6.4	4.7	4.4
R_{Bragg}	0.027	0.029	0.015	0.033
$\chi 2$	5.391	9.801	3.396	2.540

a) The space group $P6_222$ was arbitrarily chosen over $P6_422$ since absolute configuration cannot be determined by PXRD.

4. *In situ* monitoring of aging of REO with oxalic acid, ammonium oxalate or sodium oxalate

4.1. Scandium

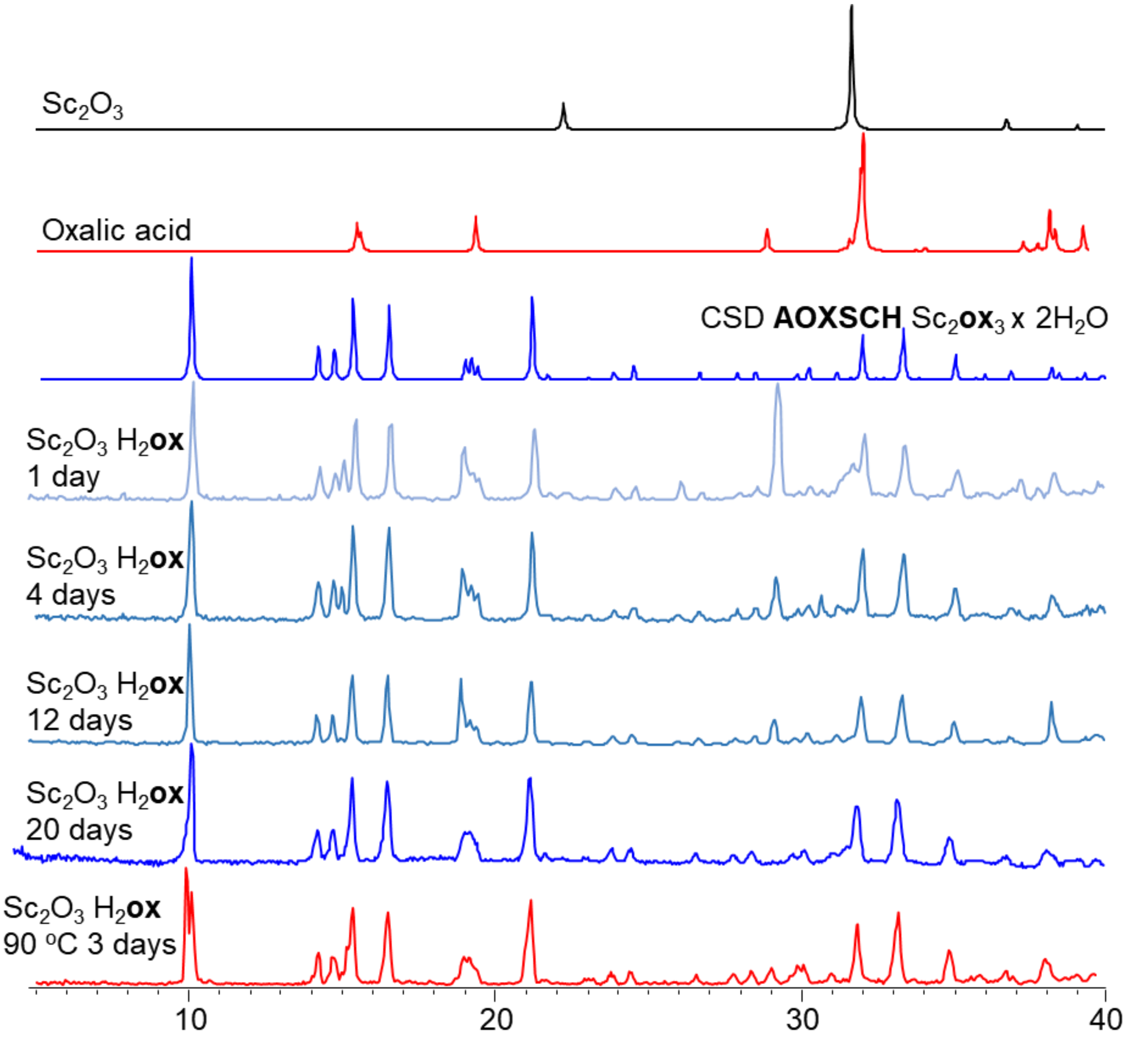

Figure S4. PXRD diffractograms of aging a mixture of Sc_2O_3 and oxalic acid in a 1:3 stoichiometric ratio, respectively.

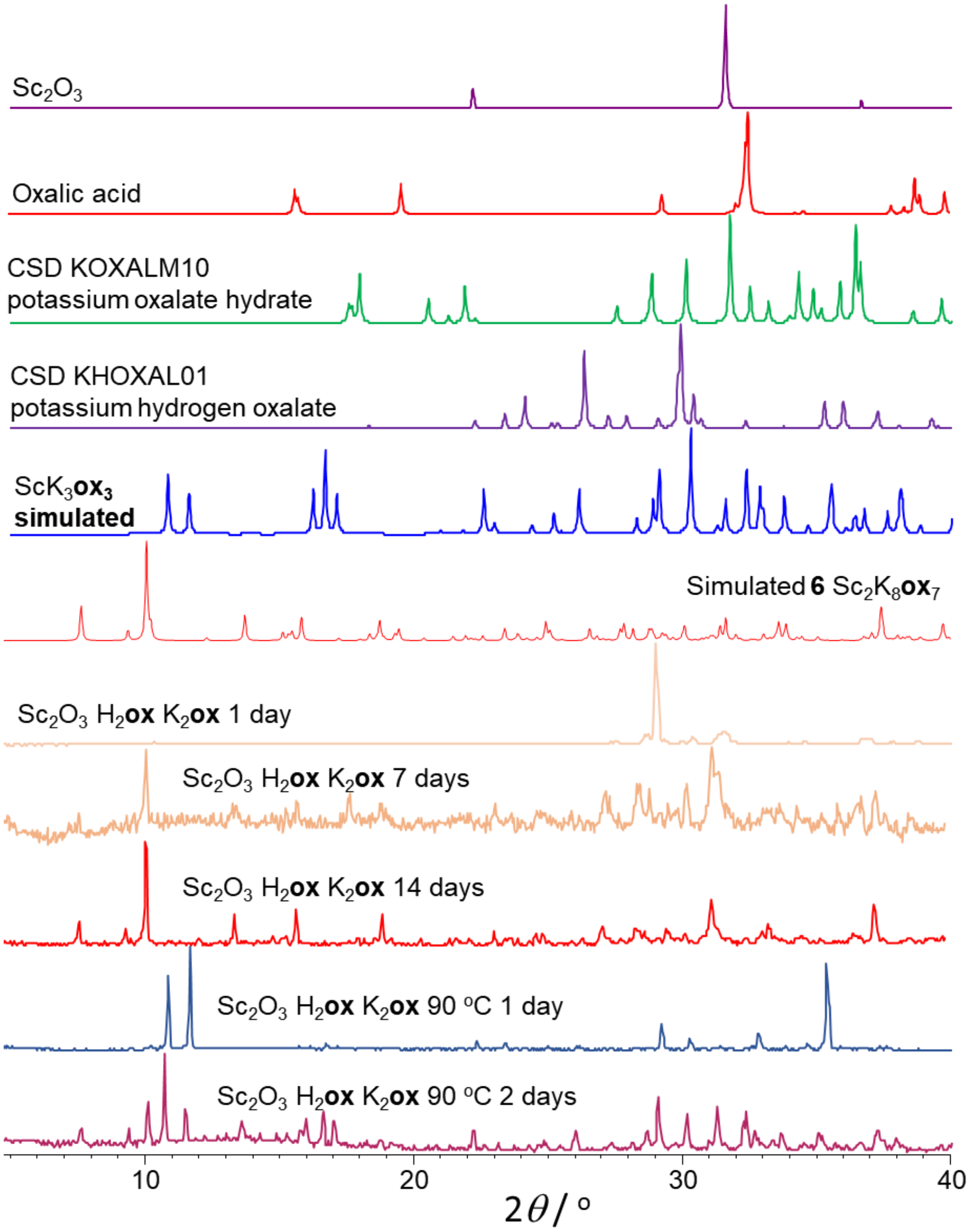

Figure S5. PXRD diffractograms of aging reaction of Sc_2O_3 with oxalic acid and potassium oxalate in a 1:3:4 stoichiometric ratio, respectively. Aging the mixture 90 ºC provides K_3Sc**ox**$_3$· $4H_2O$, an intermediate that converts to K_8Sc_2**ox**$_7$ · $10H_2O$ upon further aging. This resulting material appears to be a mixture of two phases, **5** and **6**.

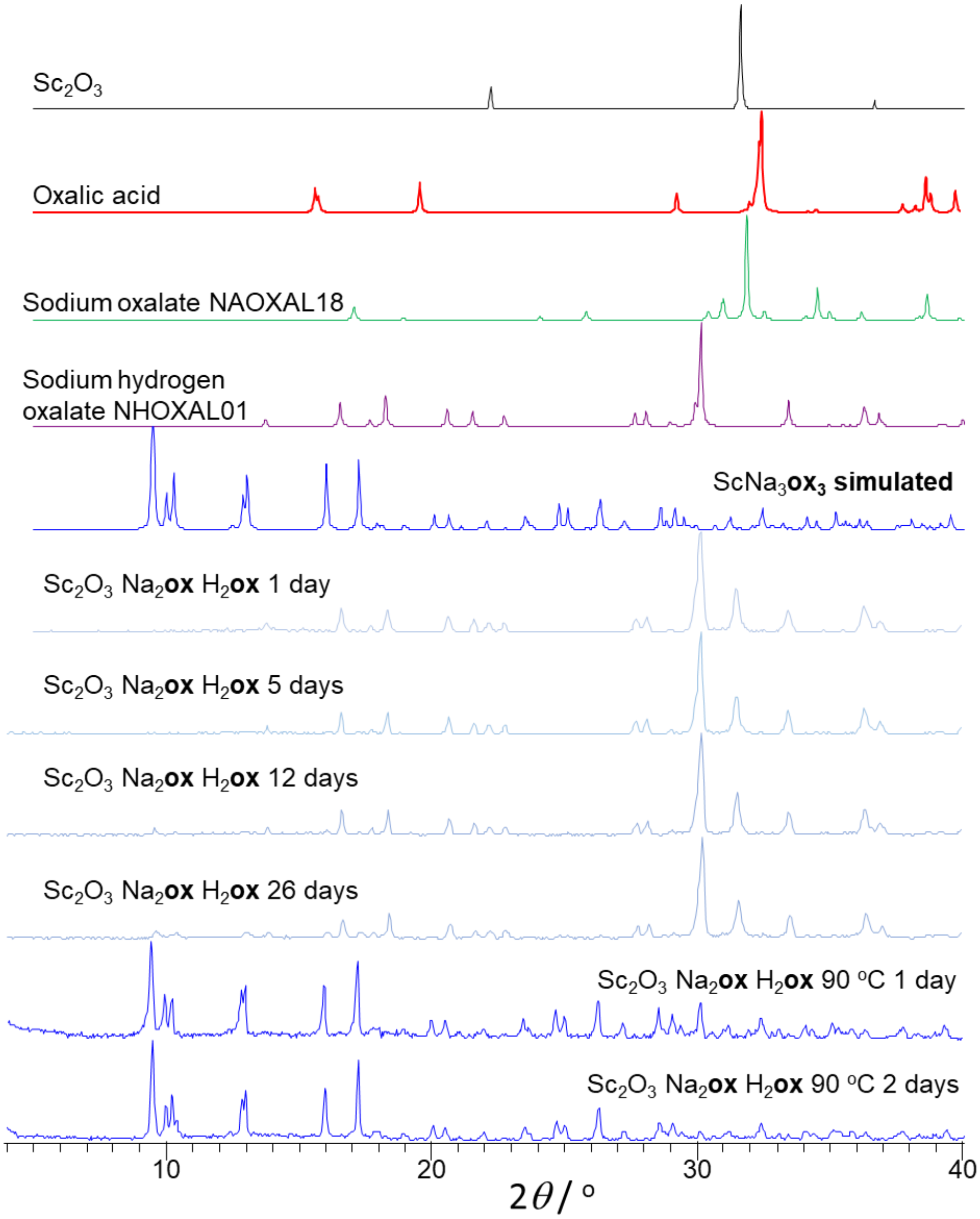

Figure S6. PXRD diffractograms of aging a mixture of Sc_2O_3, oxalic acid and sodium oxalate in a 1:3:3 stoichiometric ratio, respectively. The reaction proceeds very slowly at 45 ºC and ~96% relative humidity but goes to completion within 2 days at 90 ºC.

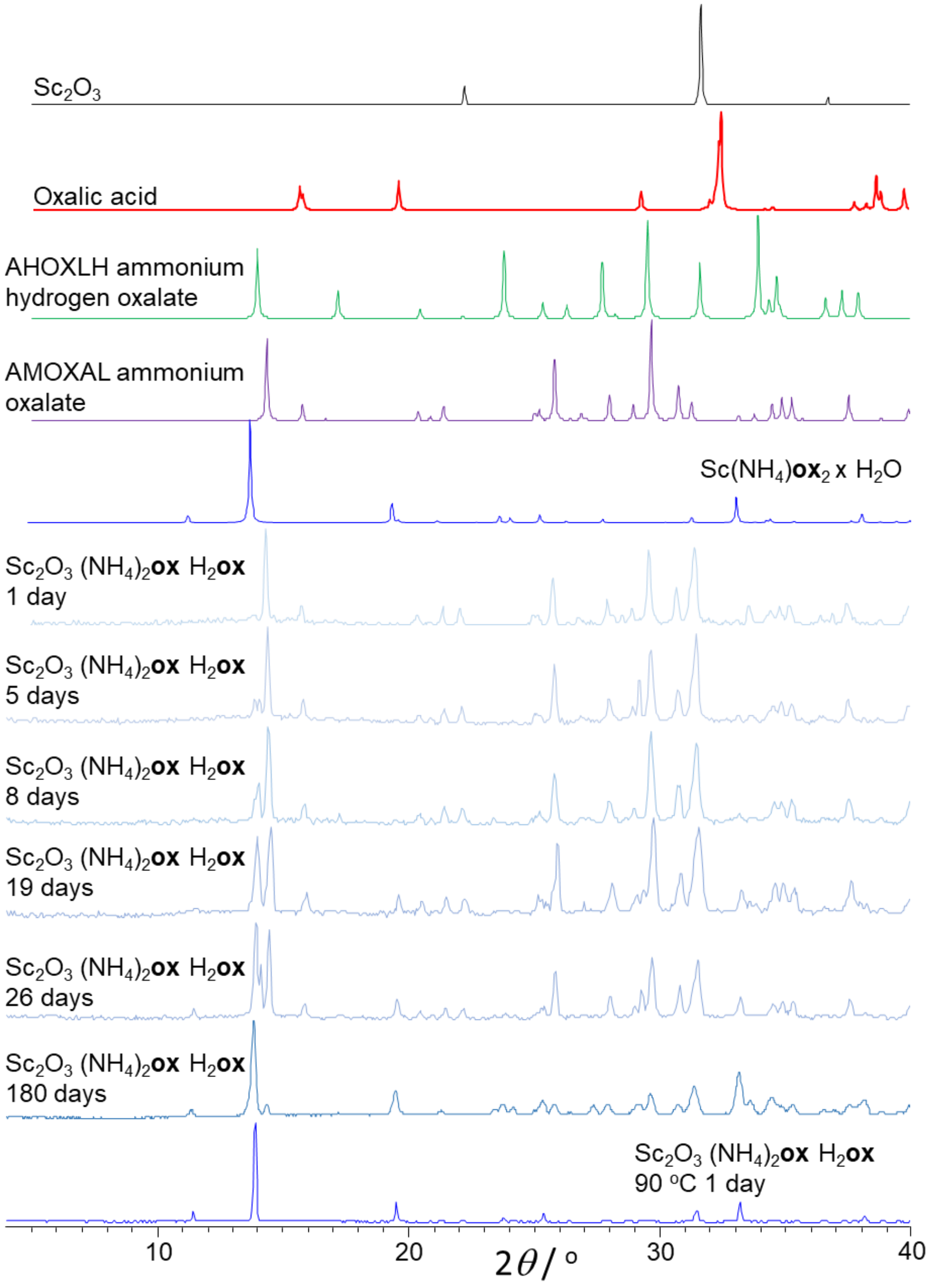

Figure S7. PXRD diffractograms of aging a mixture of Sc_2O_3, oxalic acid and ammonium oxalate in a 1:3:1 stoichiometric ratio, respectively, at 45 ºC and ~96% relative humidity. The reaction proceeds faster at 90 ºC. Structure of $(NH_4)Sc\mathbf{ox}_2 \cdot 2H_2O$ (**2**) was determined from powder data.

4.2. Ytterbium

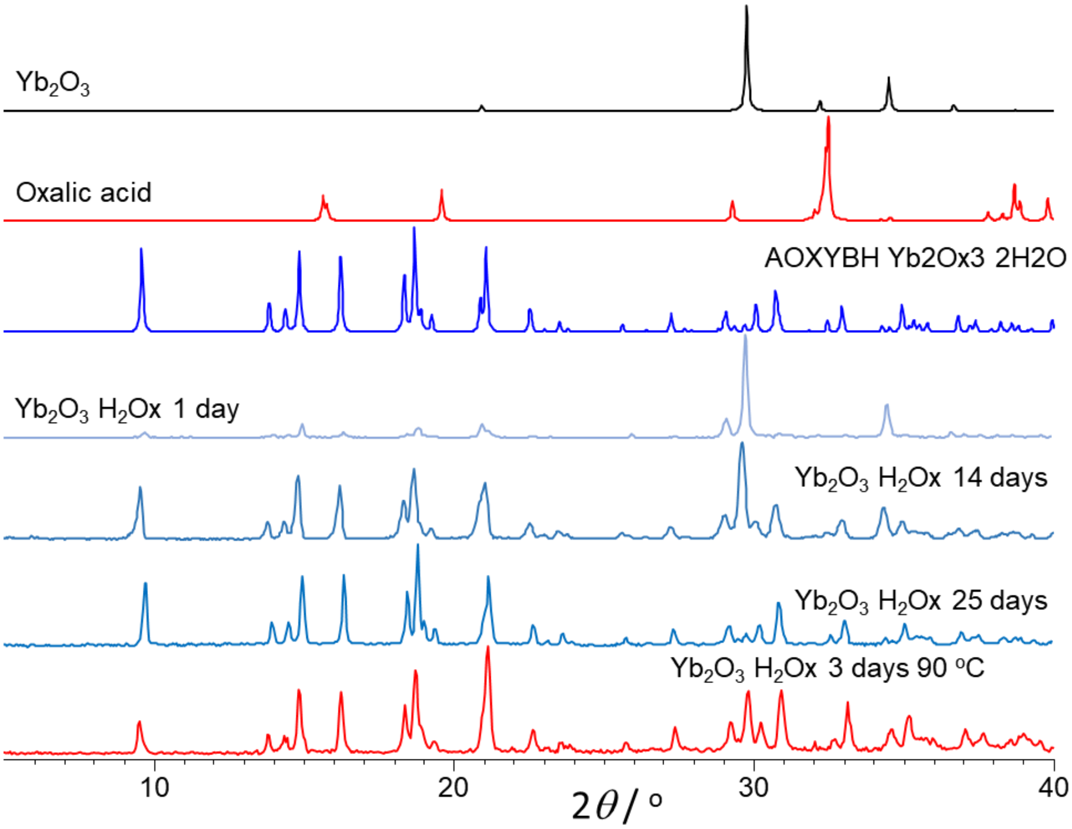

Figure S8. PXRD diffractograms of aging a mixture of Yb_2O_3 and oxalic acid in a 1:3 stoichiometric ratio, respectively at 45 ºC and ~96% RH.

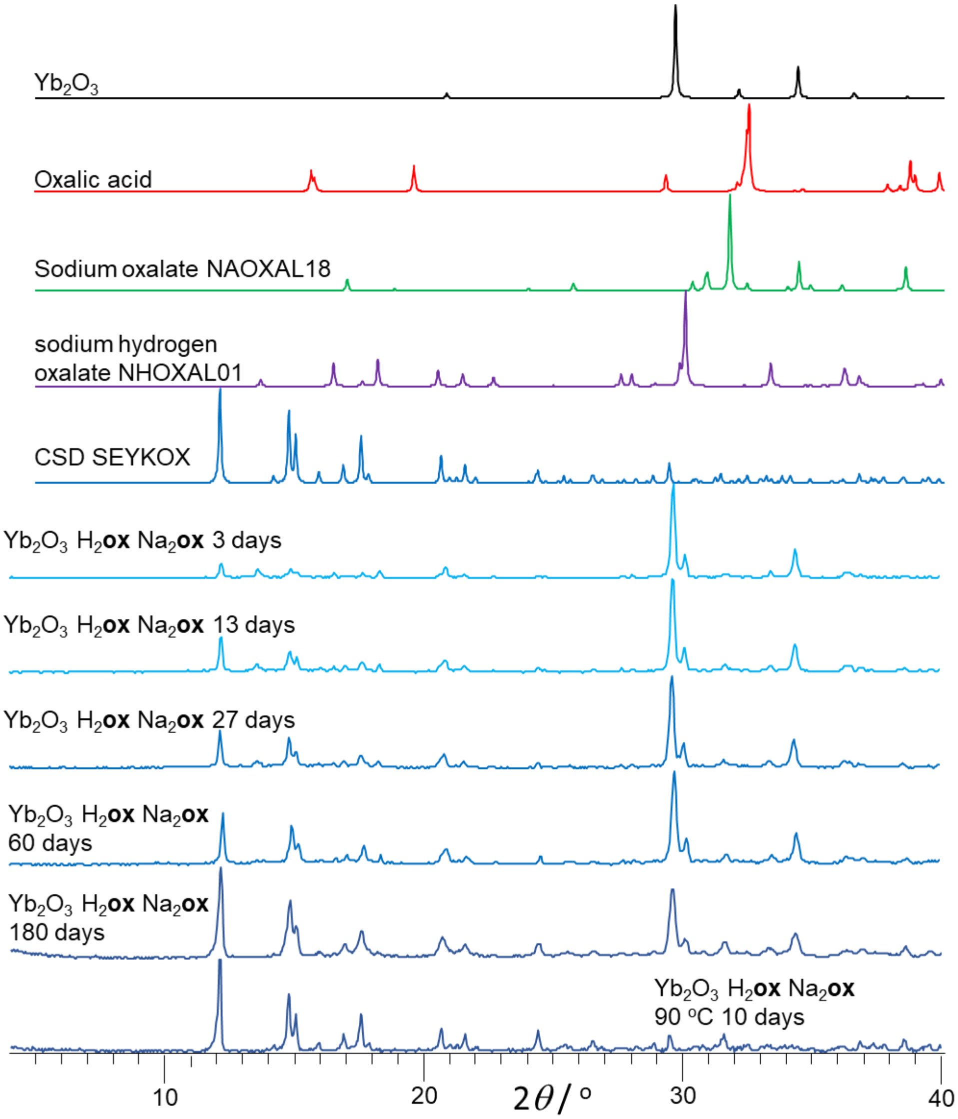

Figure S9. PXRD diffractograms of aging a mixture of Yb_2O_3, oxalic acid and sodium oxalate in a 1:3:1 stoichiometric ratio, respectively, at 45 ºC and ~96% RH. The reaction proceeds very slowly and appears to be incomplete even after 6 months of aging. Aging at 90 ºC results in the formation of the product within 5 days.

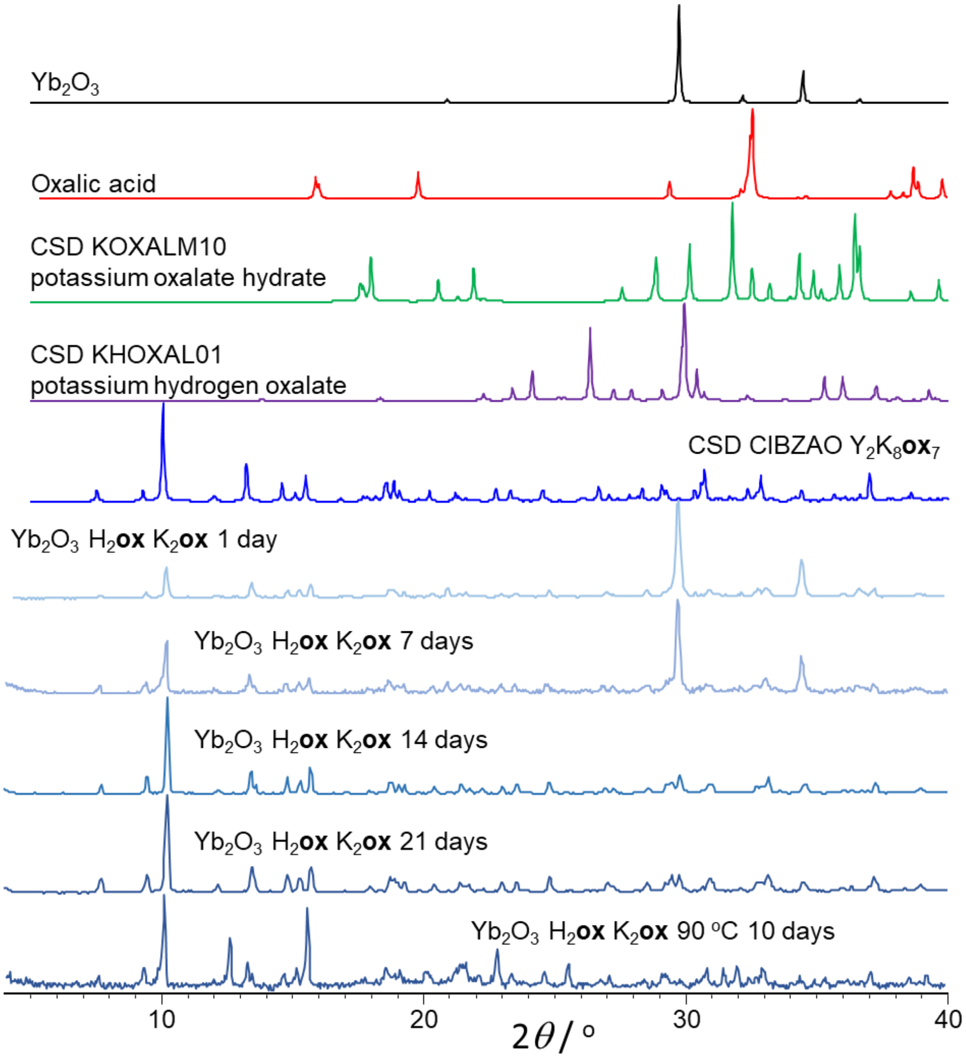

Figure S10. PXRD diffractograms of aging a mixture of Yb_2O_3, oxalic acid and potassium oxalate in a 1:3:4 stoichiometric ratio, respectively, at 45 ºC and ~96% RH. Aging the mixture at 90 ºC results in the formation of the product within 10 days.

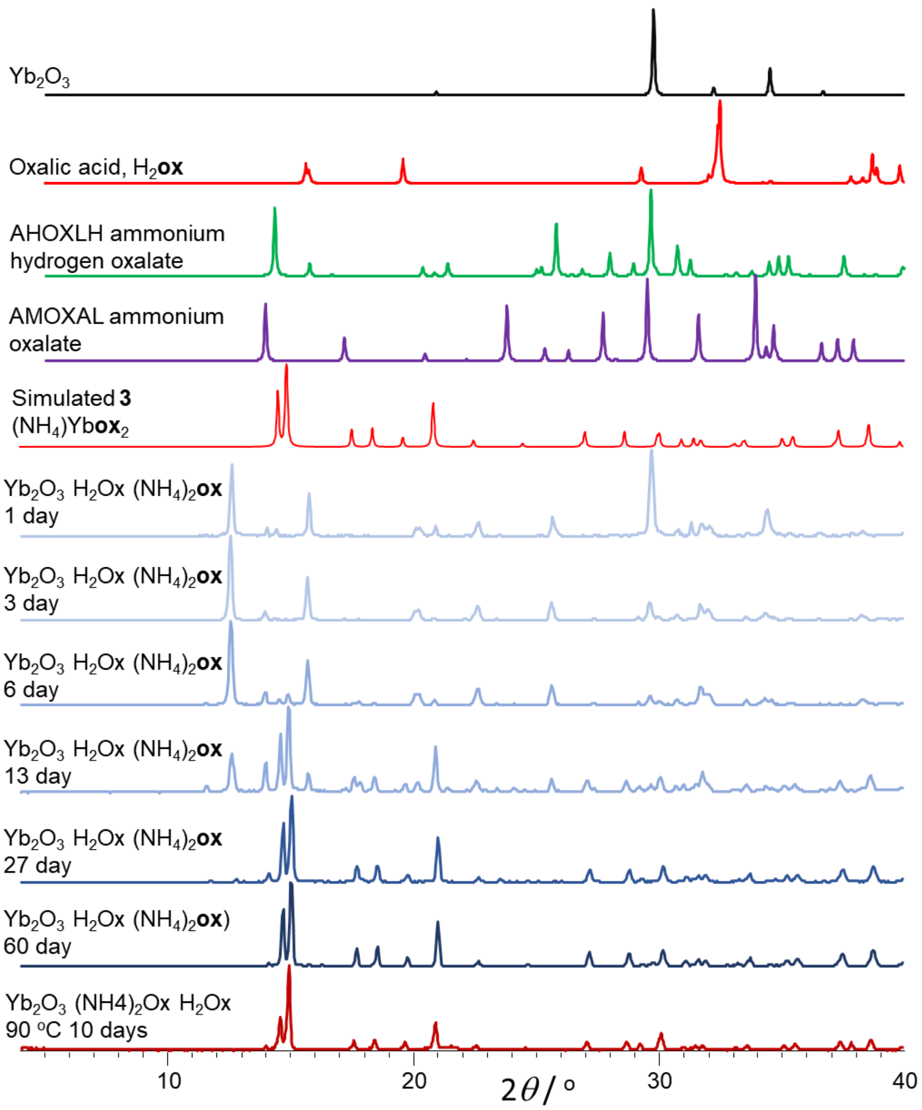

Figure S11. PXRD diffractograms of aging a mixture of Yb_2O_3, oxalic acid and ammonium oxalate in a 1:3:1 stoichiometric ratio, respectively, at 45 ºC and ~96% RH. Reaction proceeds through an as of yet unidentified intermediate phase (1 day), characterised by a strong reflection at approx. 12.5 degrees.

4.3. Lutetium

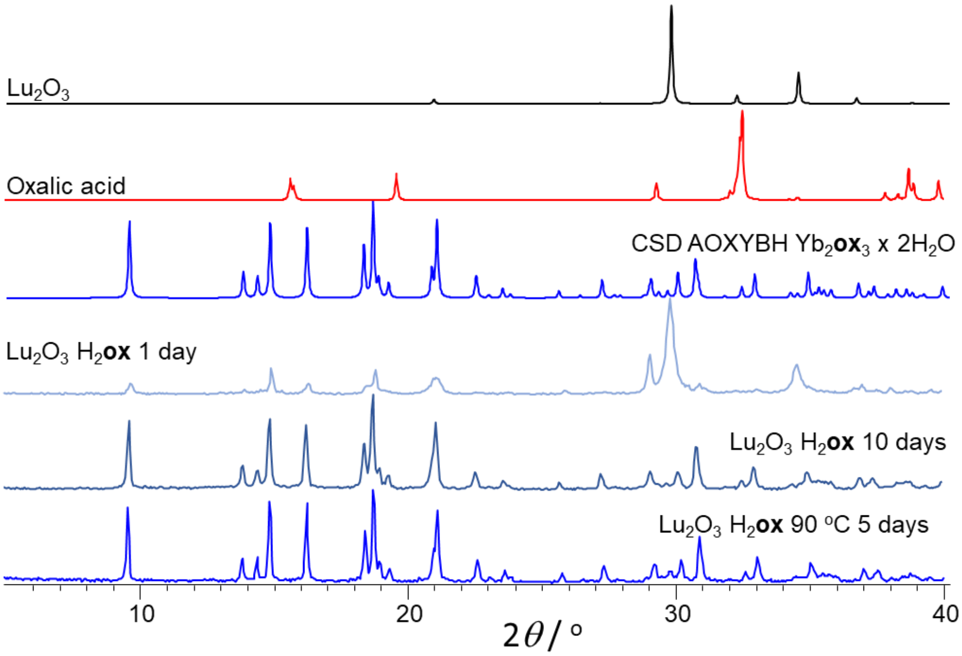

Figure S12. PXRD diffractograms of aging a mixture of Lu_2O_3 and oxalic acid in a 1:3 stoichiometric ratio, respectively, at 45 ºC and ~96% RH. Aging the mixture at 90 ºC provides the same phase within 5 days.

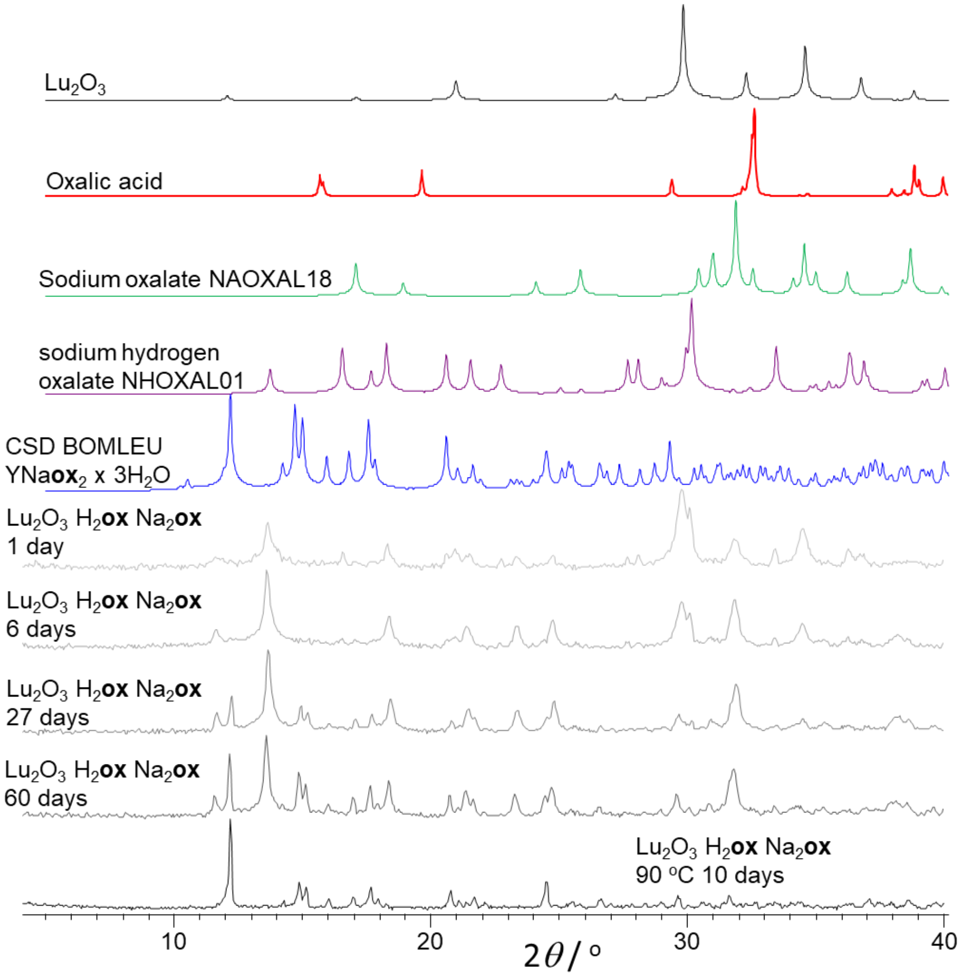

Figure S13. PXRD diffractograms of accelerated aging of a mixture of Lu_2O_3, oxalic acid and sodium oxalate in a 1:3:1 stoichiometric ratio, respectively, at 45 ºC and ~96% RH. Reaction proceeds through an as of yet unknown intermediate characterised by a prominent reflection at 13.5 2θ degrees. Aging the mixture at 90 ºC provides the material isostructural to the BOMLEU phase within 10 days. Y-axis values displayed as square root of intensity for clarity.

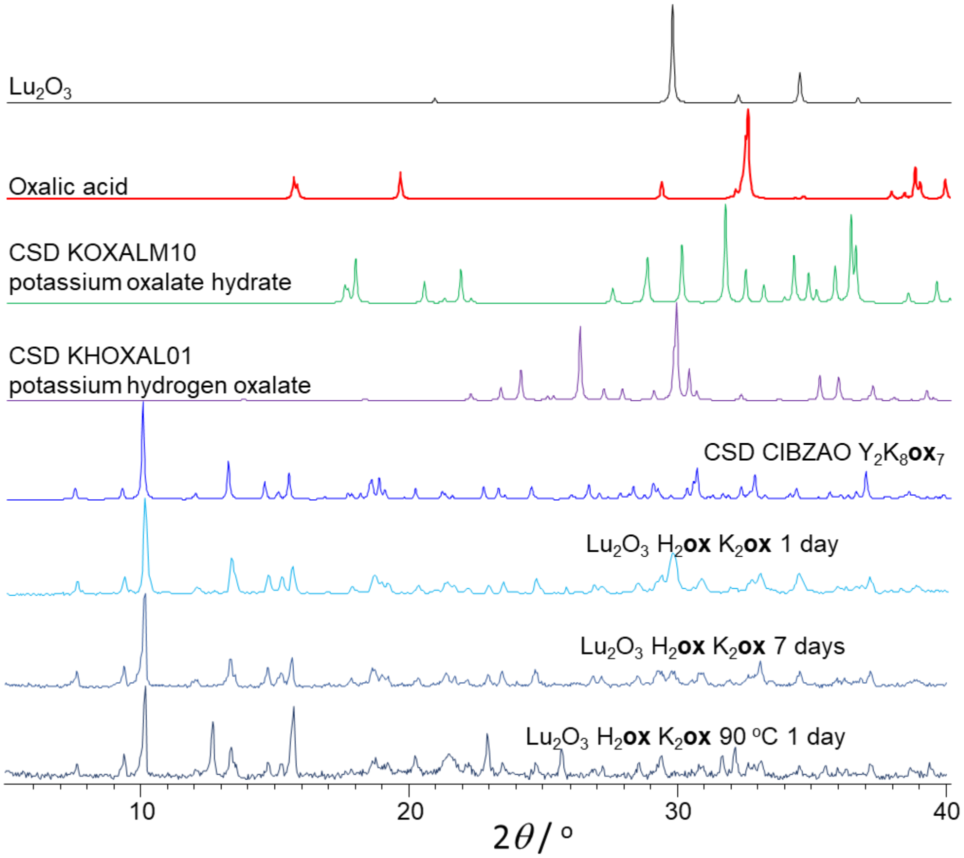

Figure S14. PXRD diffractograms of accelerated aging of a mixture of Lu_2O_3, oxalic acid and potassium oxalate in a 1:3:4 stoichiometric ratio, respectively, at 45 ºC and ~96% RH. Aging the mixture at 90 ºC provides the same phase within 1 days.

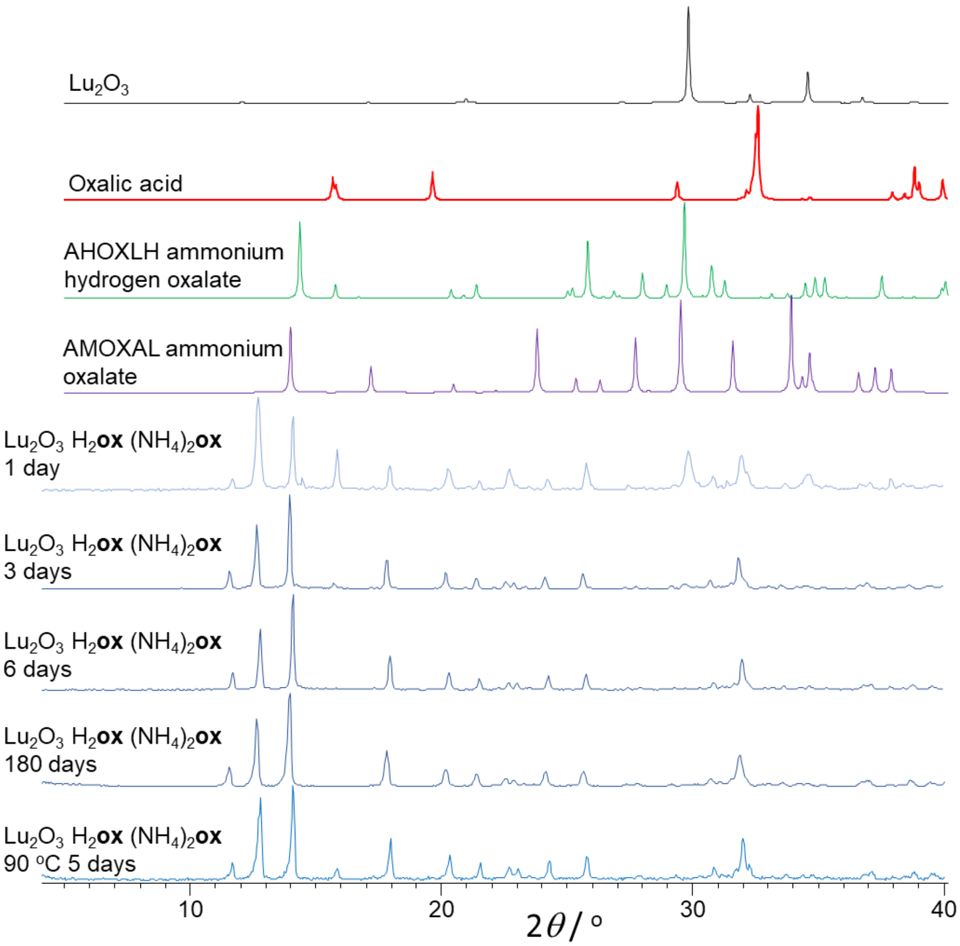

Figure S15. PXRD diffractograms of accelerated aging of a mixture of Lu_2O_3, oxalic acid and ammonium oxalate in a 1:3:3 stoichiometric ratio, respectively, at 45 ºC and 96% RH. Aging the mixture at 90 ºC provides the same product within 5 days. The product doesn't correspond or is structurally similar to any know phase.

4.4.Europium

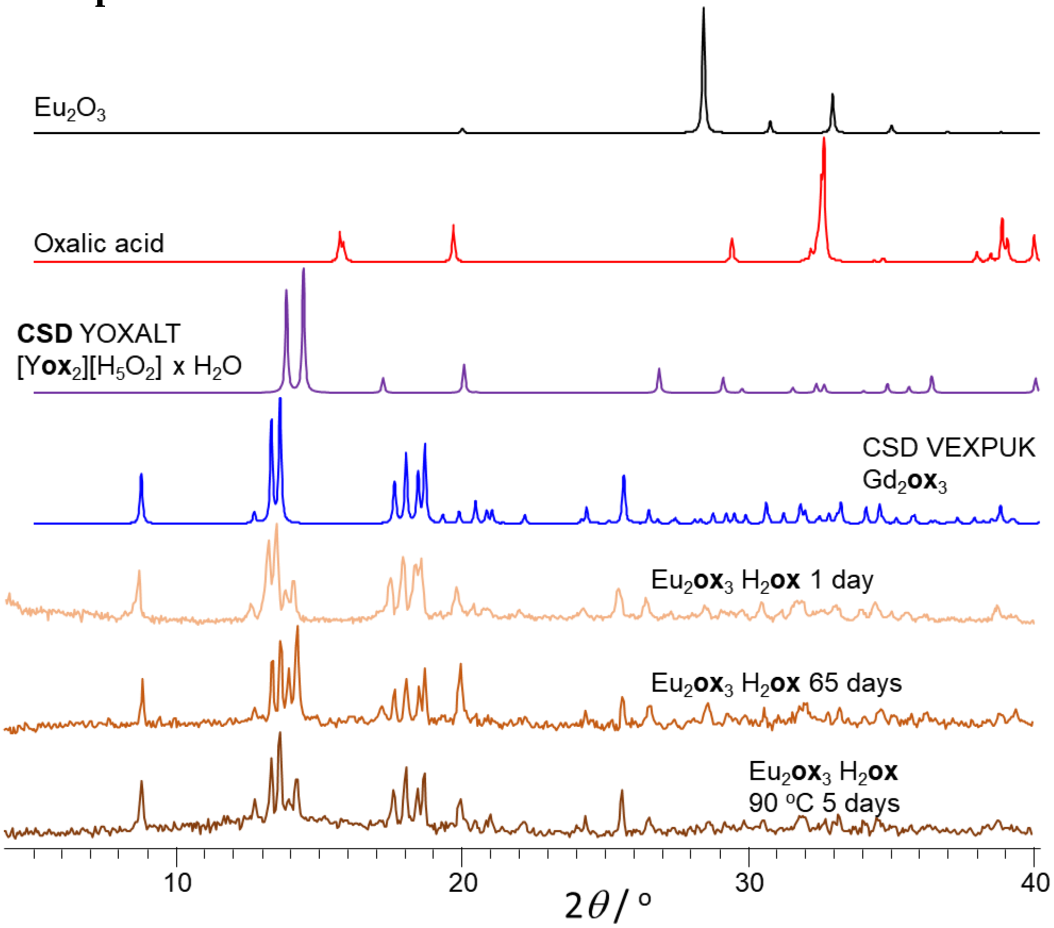

Figure S16. PXRD diffractograms of a mixture of Eu_2O_3 and oxalic acid in a 1:3 stoichiometric ratio, respectively. The product is structurally reminiscent of Gd$_2$**ox**$_3$ · 8.5H_2O (CSD VEXPUK) and [Y**ox**$_2$][H_5O_2] · H_2O (CSD YOXALT).

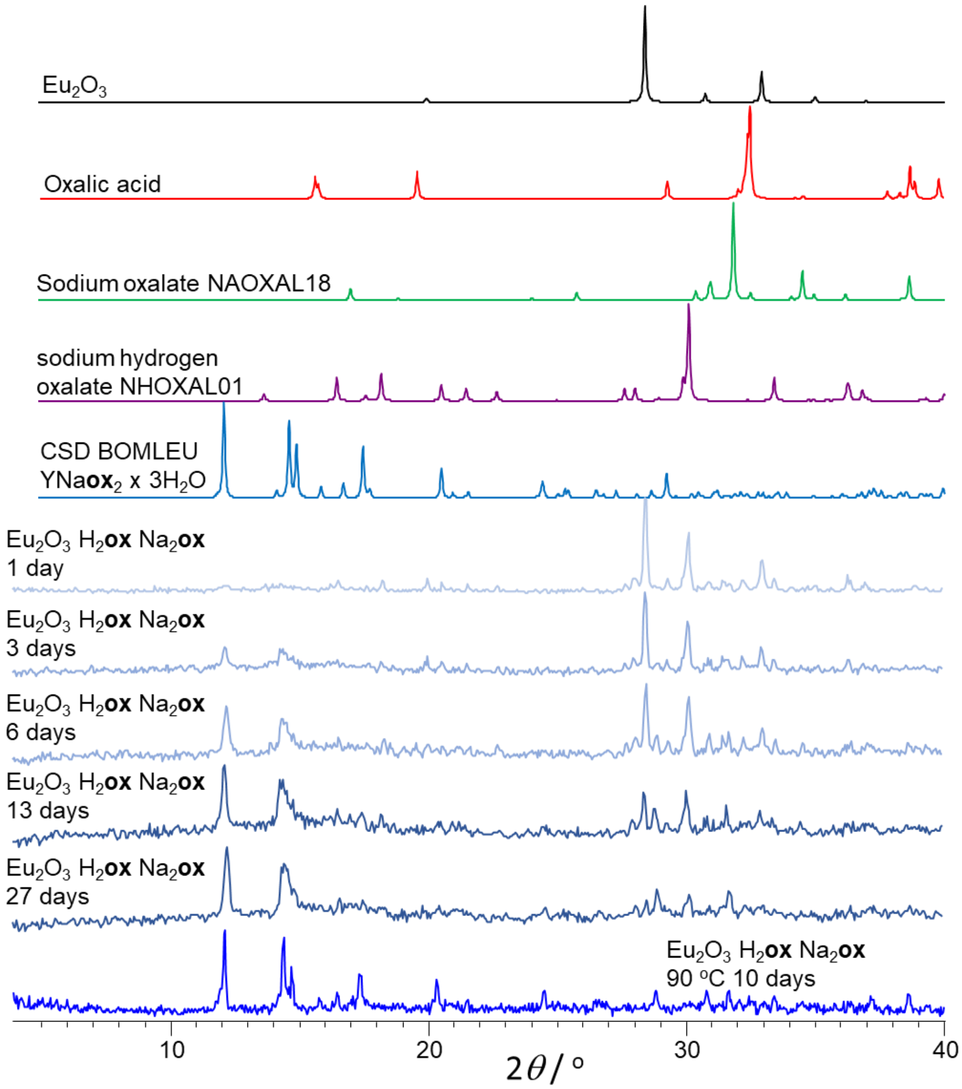

Figure S17. PXRD diffractograms of accelerated aging of a mixture of Eu_2O_3, oxalic acid and sodium oxalate in a 1:3:1 stoichiometric ratio, respectively, at 45 ºC and ~96% RH. The product is structurally reminiscent of $NaY\mathbf{ox}_2 \cdot 3H_2O$ (CSD BOMLEU). Aging at 90 ºC provides the same phase within 10 days.

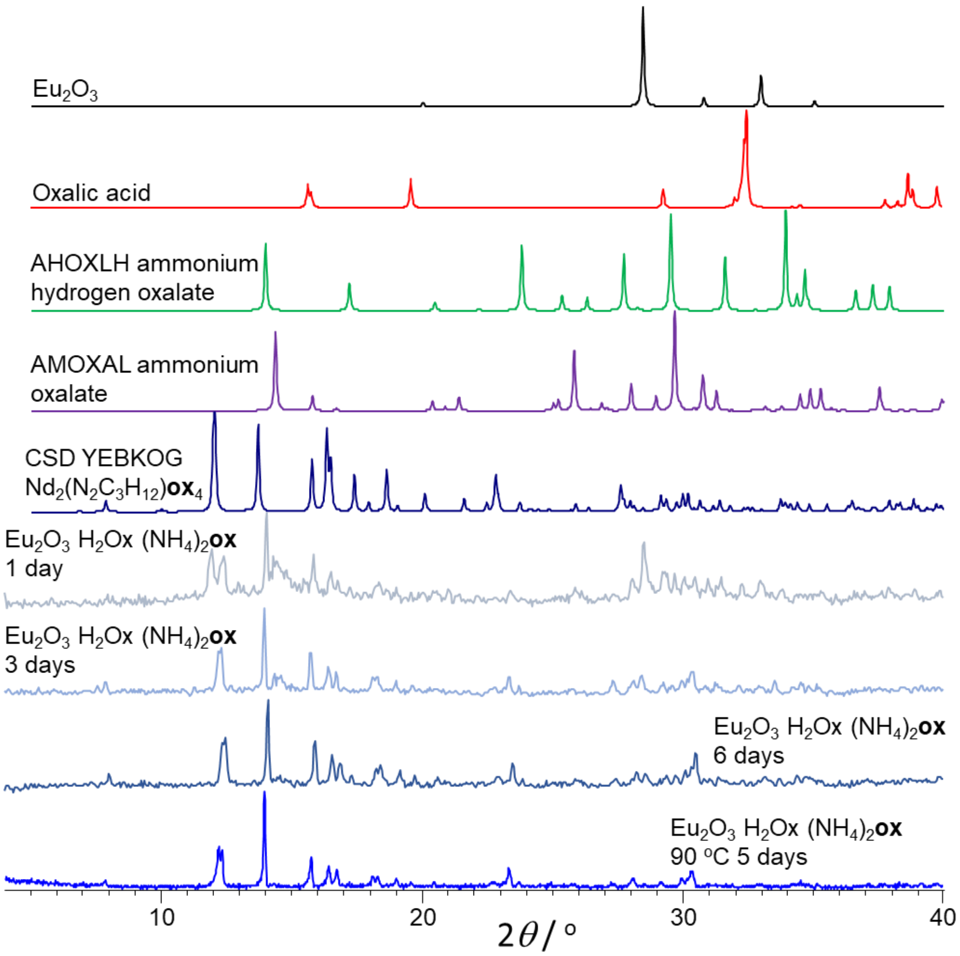

Figure S 18. PXRD diffractograms of accelerated aging of a mixture of Eu_2O_3, oxalic acid and ammonium oxalate in a 1:3:1 stoichiometric ratio, respectively, at 45 ºC and ~96% RH. The product is structurally reminiscent of $(C_3H_{12}N_2)Nd_2$**ox**$_4 \cdot 3H_2O$ (CSD YEBKOG). Aging at 90 ºC provides the same product within 5 days.

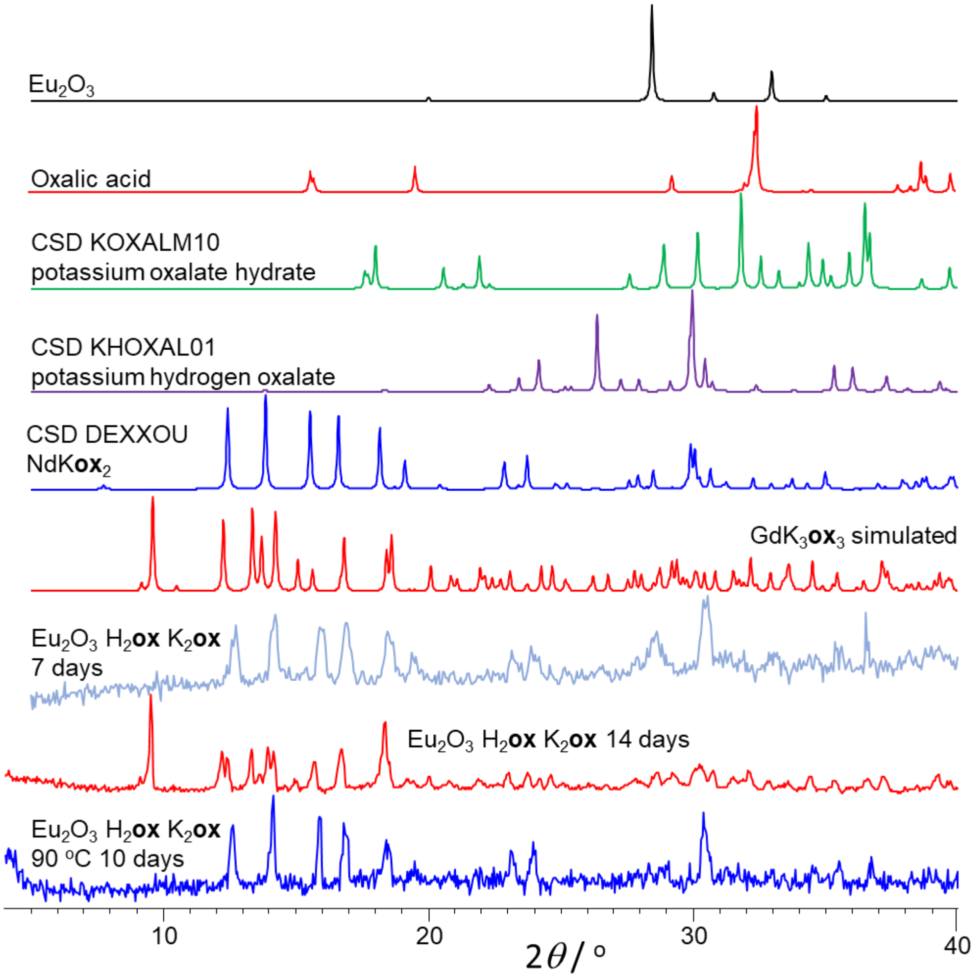

Figure S19. PXRD diffractograms of accelerated aging of a mixture of Eu_2O_3, oxalic acid and potassium oxalate in a 1:3:3 stoichiometric ratio, respectively, at 45 ºC and ~96% RH. The intermediate product is structurally reminiscent of KNd**ox**$_2$ · $3H_2O$ (CSD DEXXOU). Upon further aging the intermediate partially converts to **8**.

4.5.Lanthanum

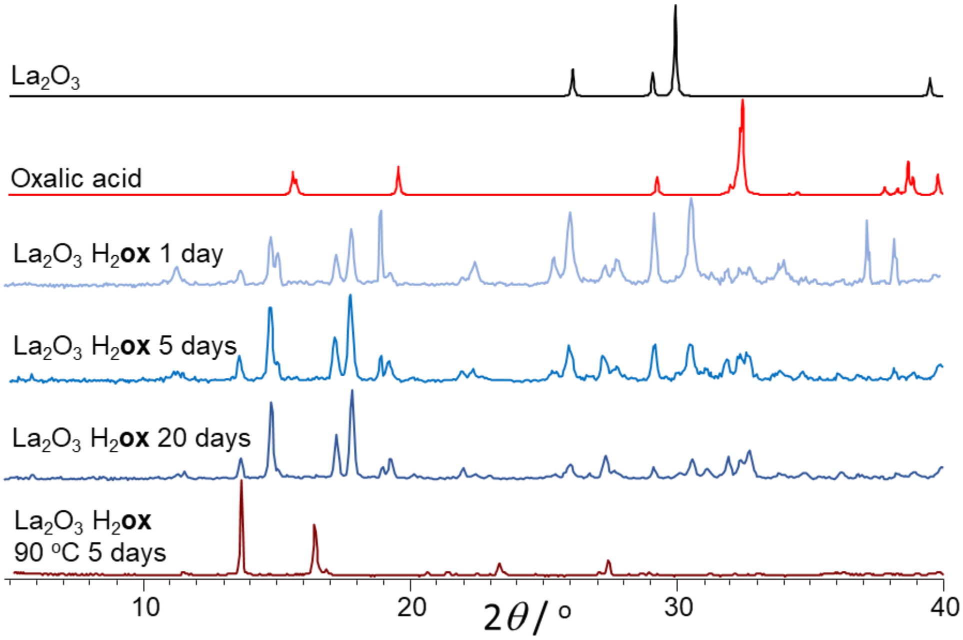

Figure S20. PXRD diffractograms of accelerated aging at 45 ºC and 96% RH of a mixture of La_2O_3 and oxalic acid in a 1:3 stoichiometric ratio, respectively. The structures of both the product and the apparent intermediate are as of yet unknown. Aging the mixture at 90 ºC provides an unknown phase.

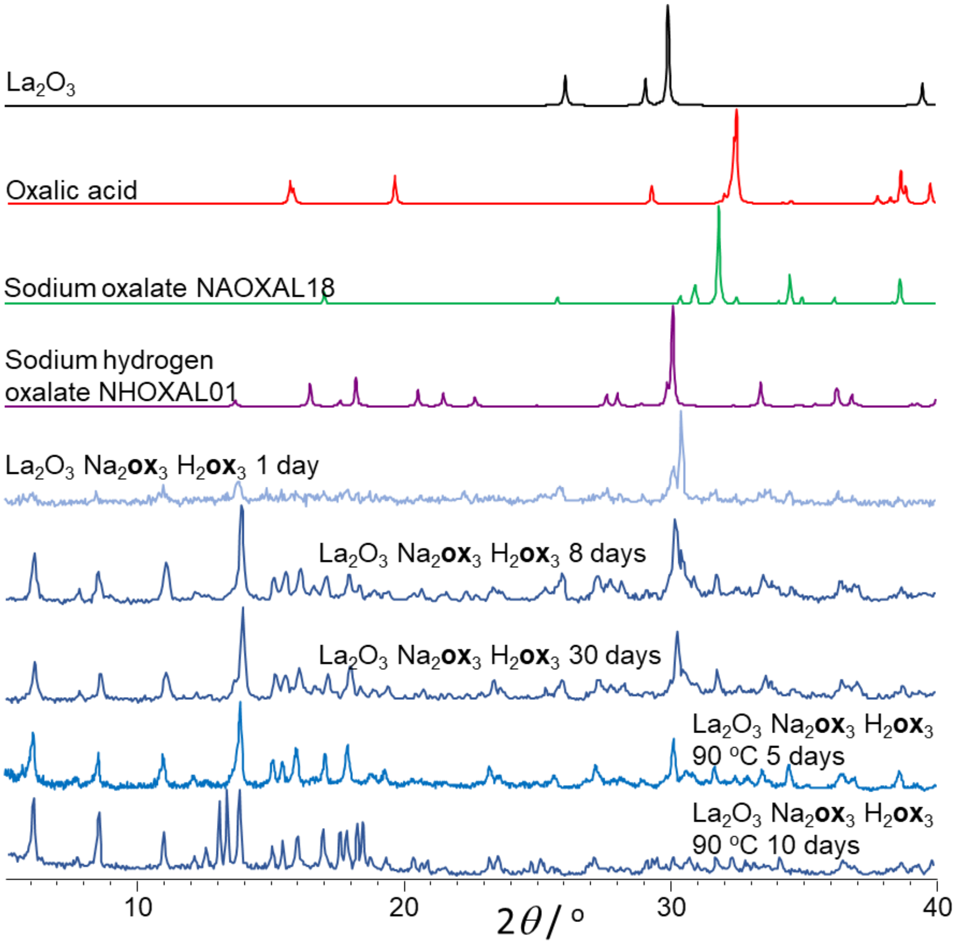

Figure S21. PXRD diffractograms of accelerated aging at 45 ºC and 96% RH of a mixture of La_2O_3, oxalic acid and sodium oxalate in a 1:3:3 stoichiometric ratio, respectively. The crystal structure of the product is unknown. Aging at 90 ºC produces the same unknown phase after 5 days. Upon further aging in the same conditions, a new phase, or a mixture of phases is formed.

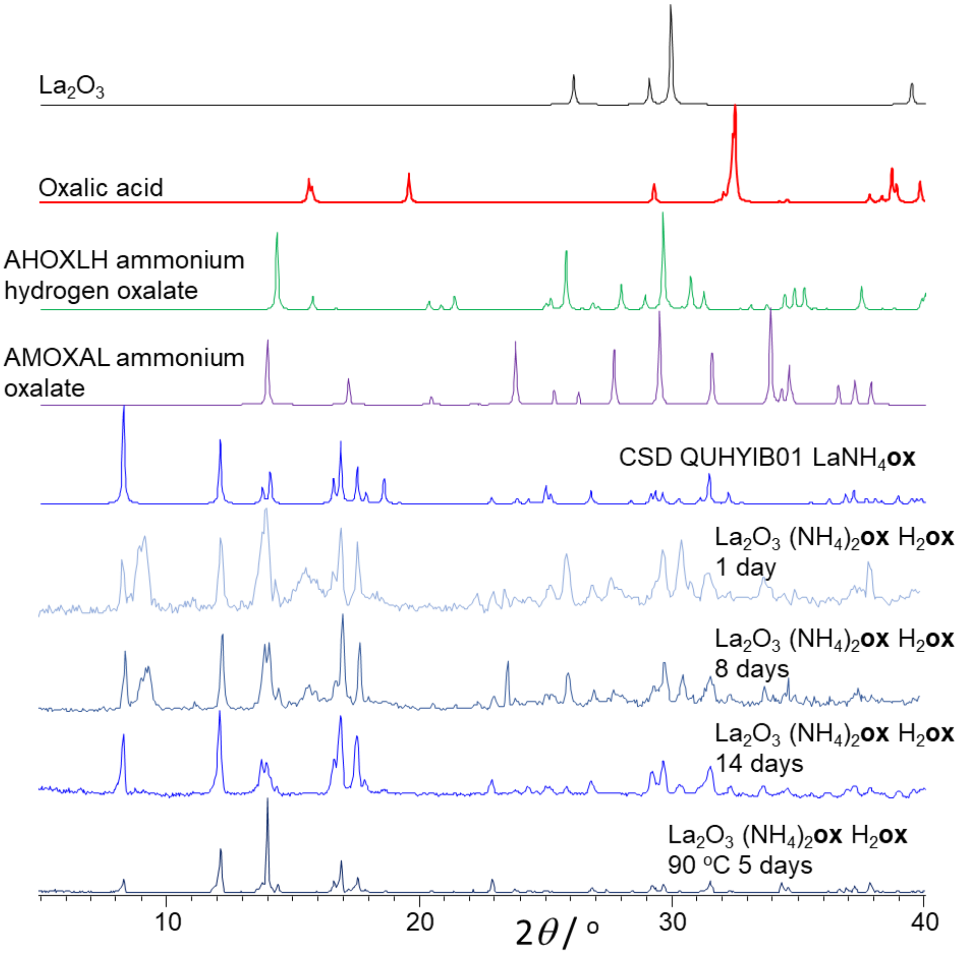

Figure S22. PXRD diffractograms of accelerated aging at 45 ºC and 96% RH of a mixture of La_2O_3, oxalic acid and ammonium oxalate in a 1:3:1 stoichiometric ratio, respectively. The crystal structure of the product corresponds to CSD QUHYIB01. An unknown intermediate phase is formed during aging, as evident from PXRD patterns (1 and 8 days). Aging the same mixture at 90 ºC seemingly provides the same phase, but with a higher degree of preferred crystallite orientation.

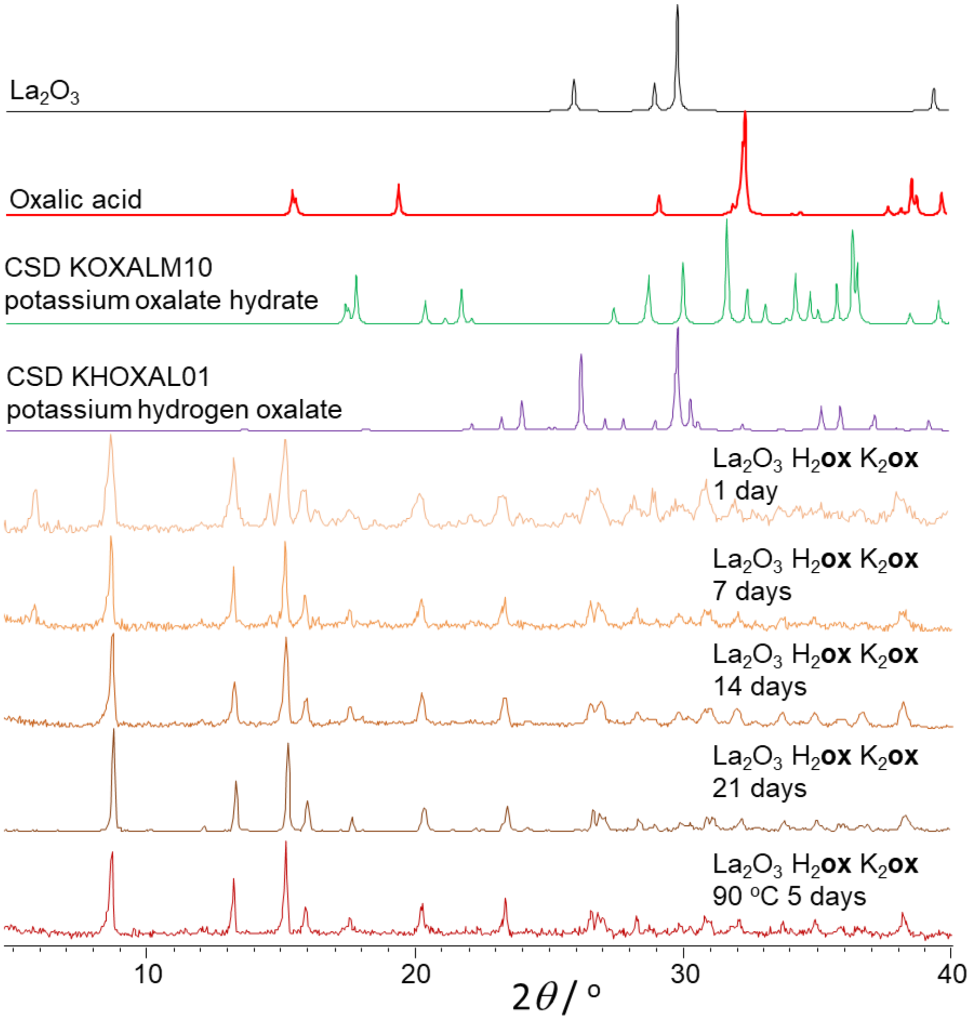

Figure S23. PXRD diffractograms of accelerated aging at 45 ºC and 96% RH of a mixture of La_2O_3, oxalic acid and potassium oxalate in a 1:3:3 stoichiometric ratio, respectively. The crystal structure of the product is unknown. Aging the mixture at 90 ºC provides the same unknown phase.

4.6. Yttrium

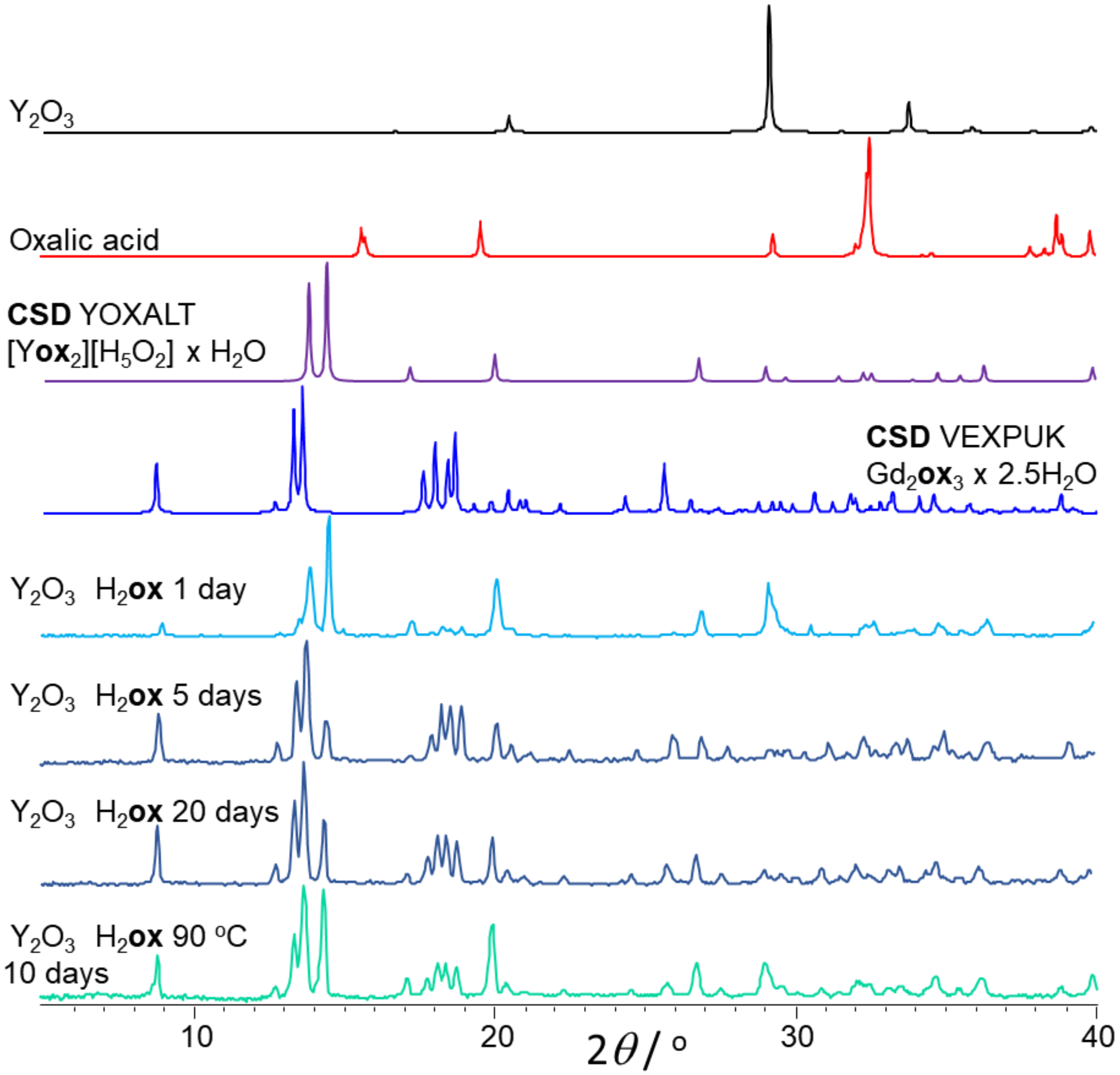

Figure S24. PXRD diffractograms of aging a mixture of Y_2O_3 and oxalic acid in a 1:3 stoichiometric ratio, respectively, at 45 ºC and ~96% RH. The reaction proceeds through an intermediate structurally similar to [Y**ox**$_2$][H_5O_2] · H_2O (CSD YOXALT) but ends up as a mixture of two phases, presumably YOXALT and yttrium analogue of VEXPUK.

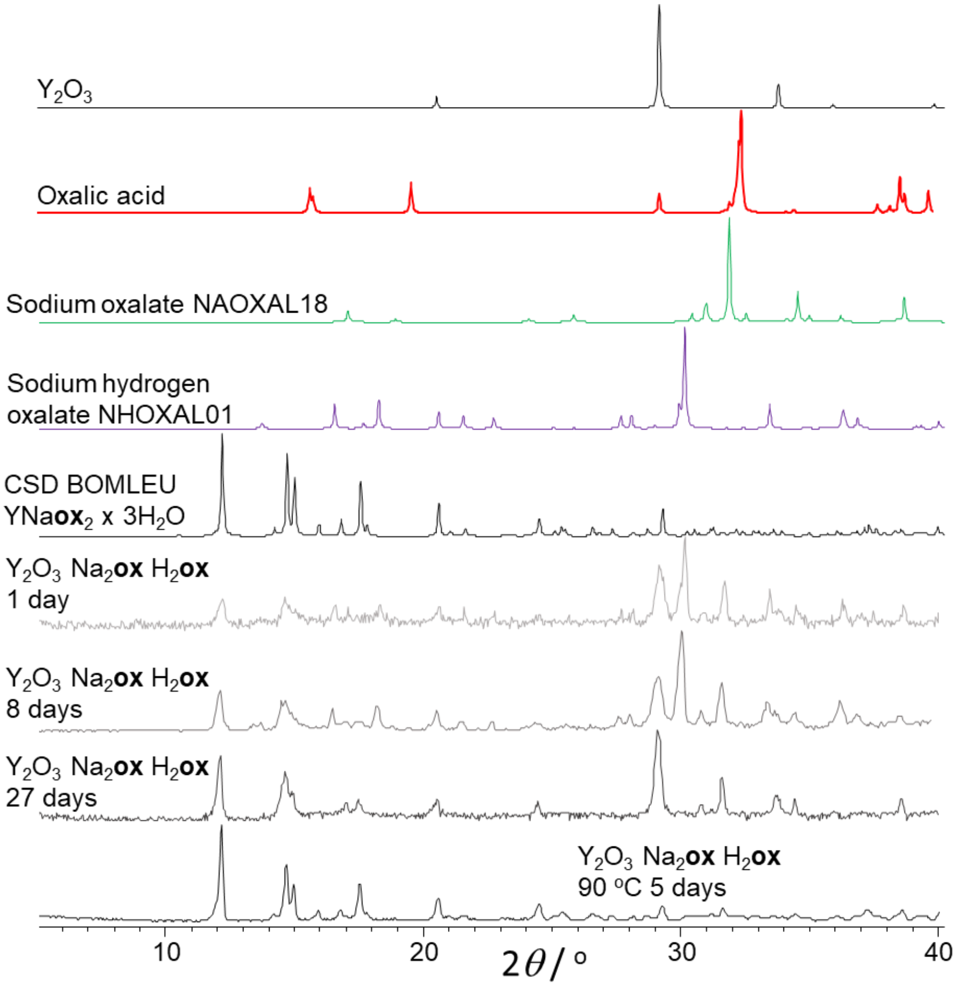

Figure S25. PXRD diffractograms of accelerated aging at 45 ºC and ~96% RH of Y_2O_3, oxalic acid and sodium oxalate in a 1:3:1 stoichiometric ratio, respectively, at 45 ºC and ~96% RH. The reaction proceeds very slowly at 45 ºC but goes to completion in 5 days at 90 ºC.

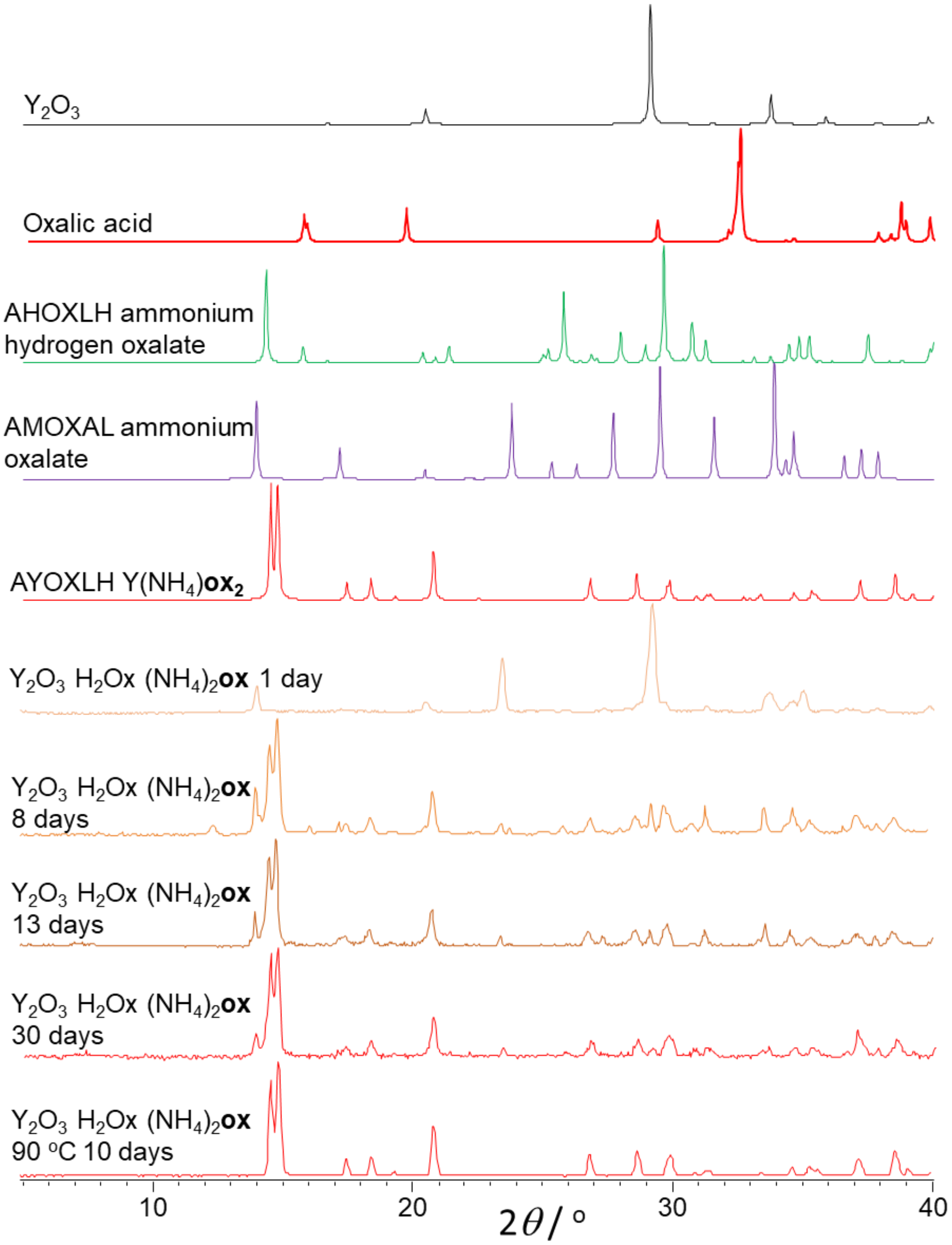

Figure S26. PXRD diffractograms of accelerated aging of Y_2O_3, oxalic acid and ammonium oxalate in a 1:3:1 stoichiometric ratio, respectively, respectively, at 45 ºC and ~96% RH. The reaction that is almost complete in 30 days at 45 ºC is complete within 10 days at 90 ºC.

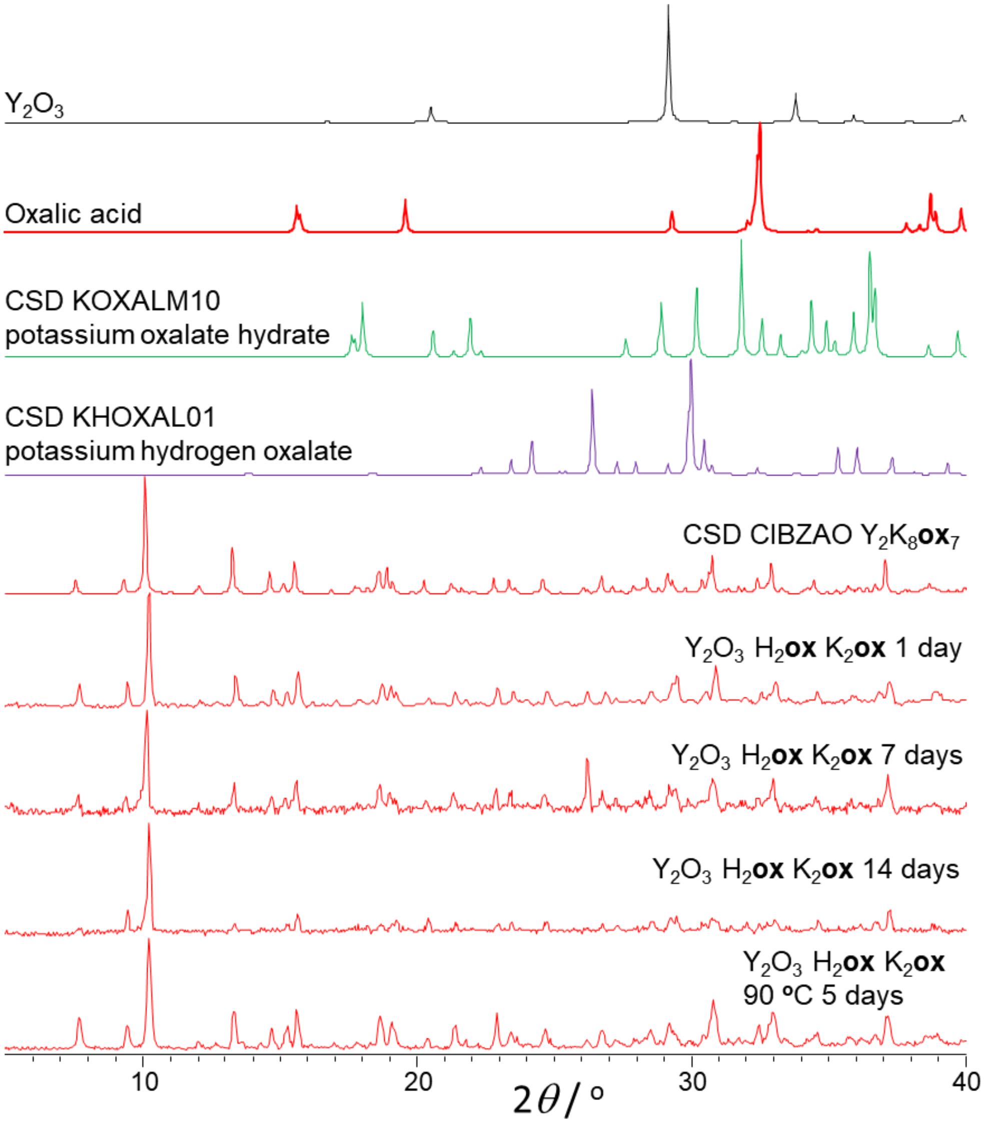

Figure S28. PXRD diffractograms of accelerated aging of a mixture of Y_2O_3, oxalic acid and potassium oxalate in a 1:4:3 stoichiometric ratio, respectively, respectively, at 45 ºC and ~96% RH. The crystal structure of the product obtained by aging at 45 ºC or 90 ºC corresponds to the structure of K_8Y_2**ox**$_7\cdot 14H_2O$ (CSD code CIBZAO).

4.7.Neodymium

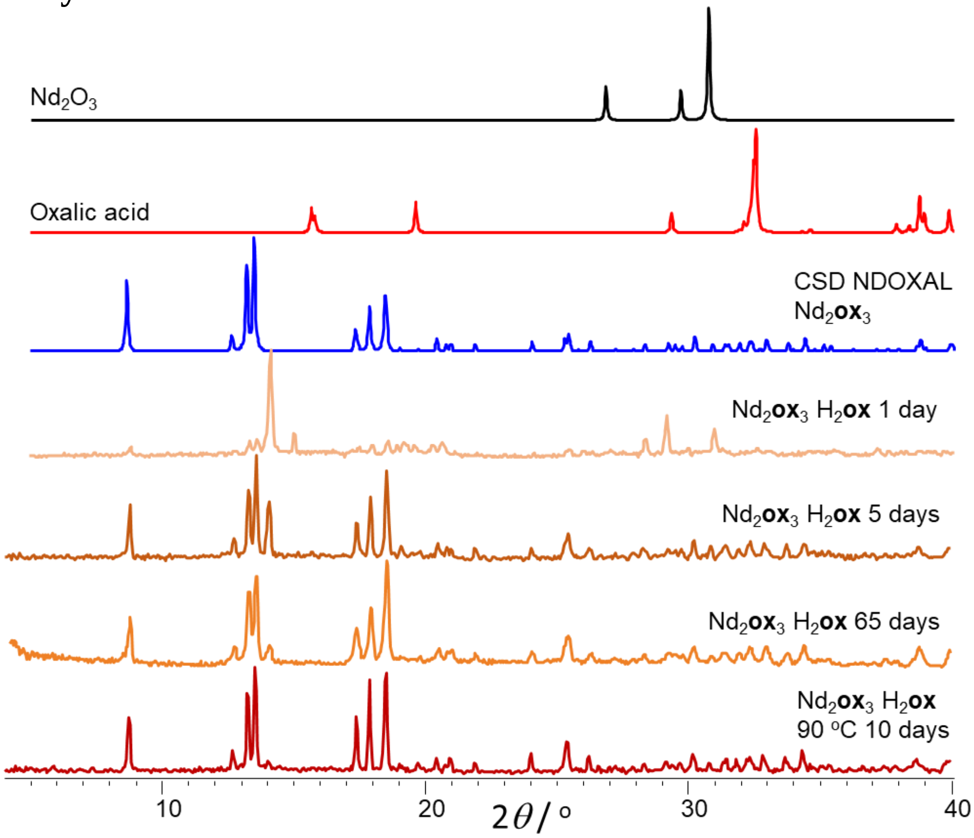

Figure S27. PXRD diffractograms of accelerated aging of a mixture of Nd_2O_3 and oxalic acid in a 1:3 stoichiometric ratio, respectively, at 45 ºC and ~96% RH. The resulting product has the structure of CSD entry NDOXAL, but the product is formed through an unknown intermediate identified by a strong Bragg reflection at 14.1 2θ degrees. Reaction at 90 ºC produces the same NDOXAL material.

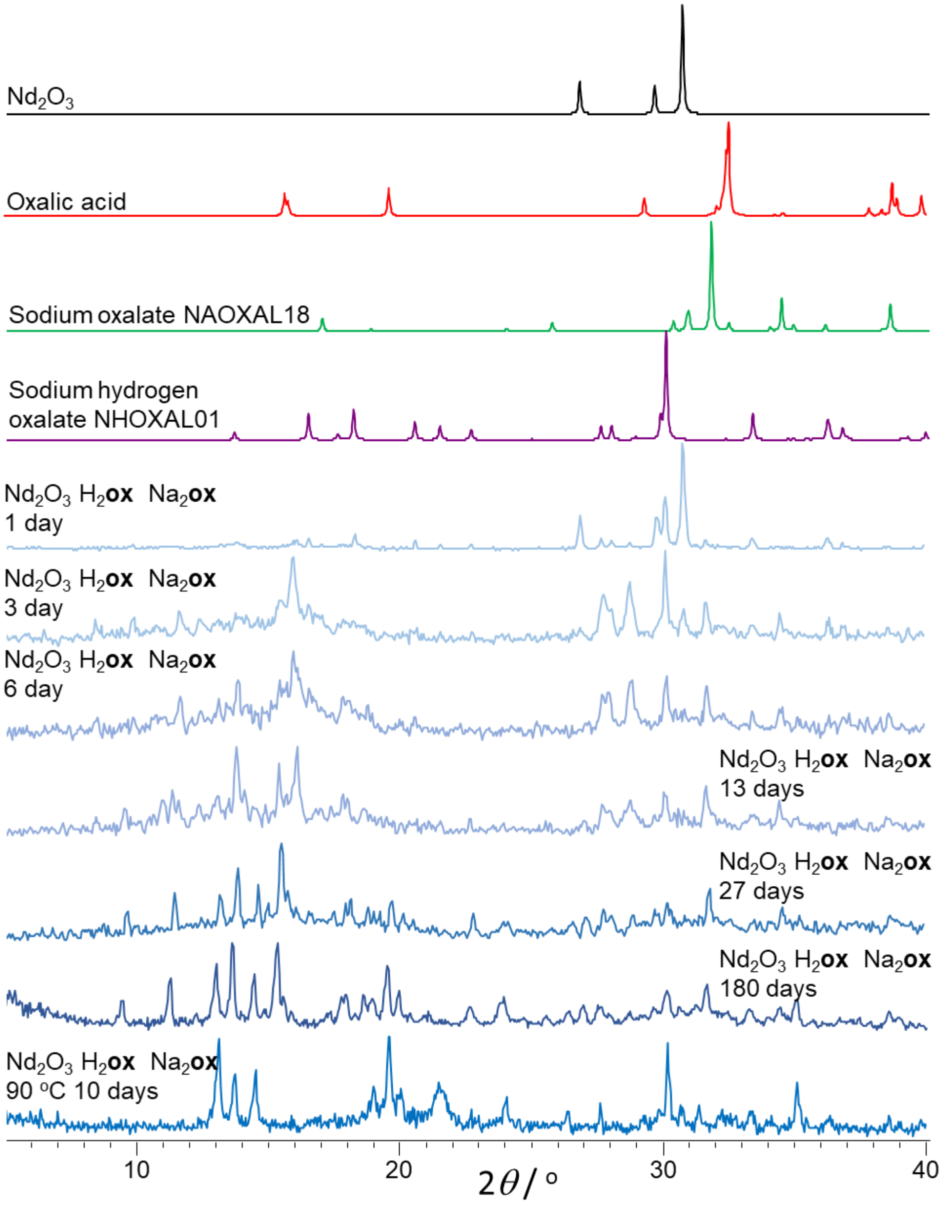

Figure S28. PXRD diffractograms of accelerated aging of a mixture of Nd_2O_3, oxalic acid and sodium oxalate in a 1:3:3 stoichiometric ratio, respectively, at 45 ºC and ~96% RH. The crystal structure of the product does not correspond to any known phase.

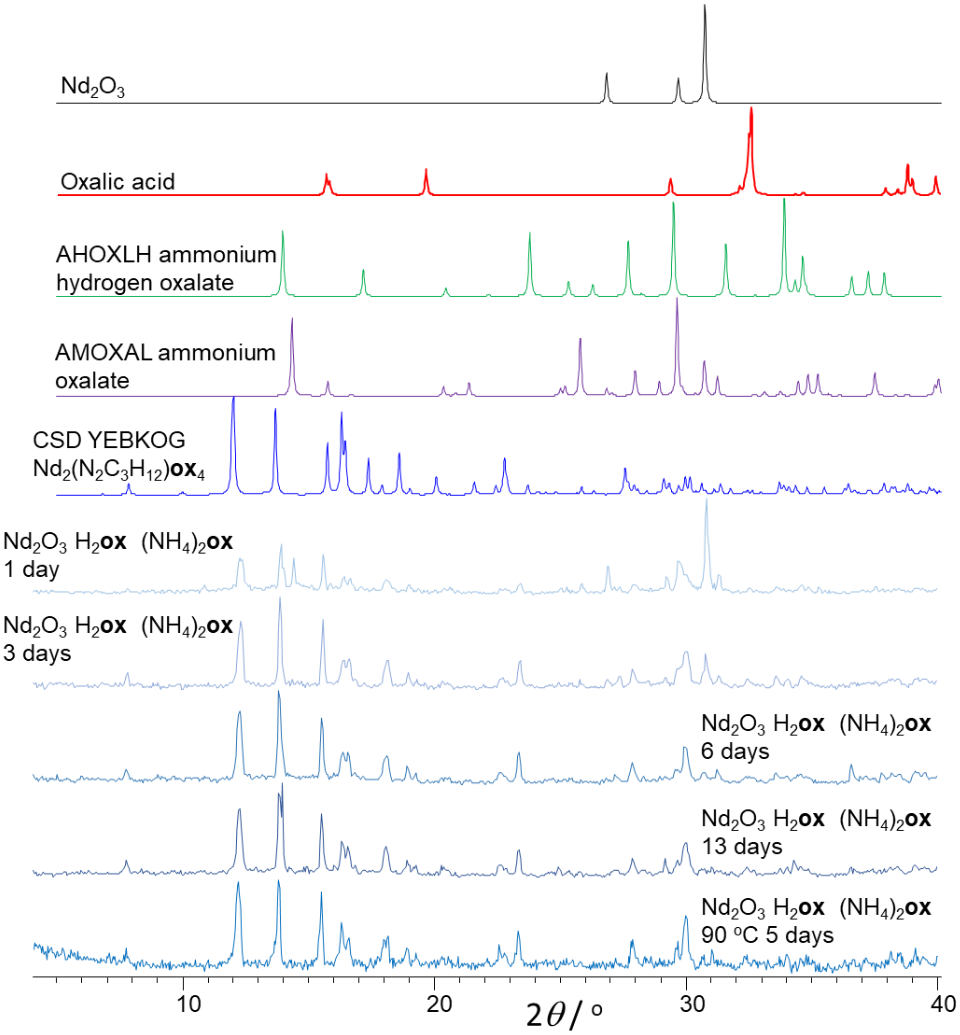

Figure S29. PXRD diffractograms of accelerated aging of a mixture of Nd_2O_3, oxalic acid and ammonium oxalate in a 1:3:1 stoichiometric ratio, respectively, at 45 ºC and 96% RH. The product is structurally reminiscent of $(C_3H_{12}N_2)Nd_2$**ox**$_4 \cdot 3H_2O$ (CSD YEBKOG). Aging the mixture at 90 ºC produces the same material.

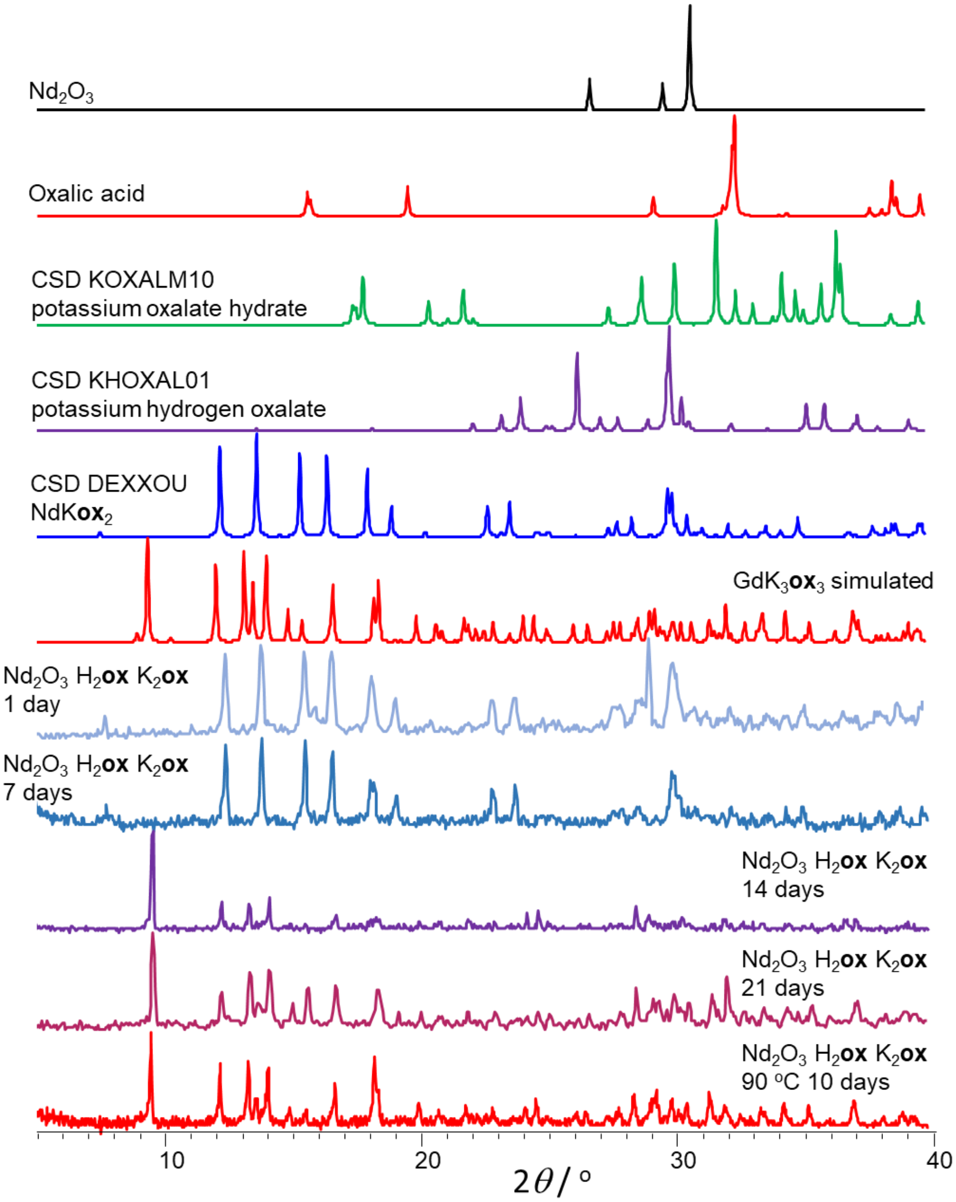

Figure S30. PXRD diffractograms of accelerated aging of a mixture of Nd_2O_3, oxalic acid and potassium oxalate in a 1:3:3 stoichiometric ratio, respectively, at 45 ºC and 96% RH. The intermediate product corresponds to KNd**ox**$_2\cdot3H_2O$ (CSD DEXXOU). Upon further aging the intermediate converts to a structure reminiscent of **7**. Aging the mixture at 90 ºC produces material analogous to 7.

5. ICP analysis

5.1. Calibration curves

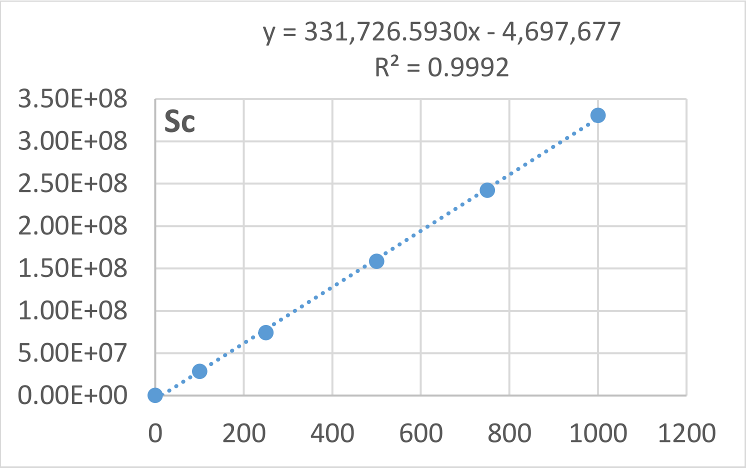

Figure S31. ICP calibration curve for scandium. Values on the abscissa axis represent mass fraction in ppb.

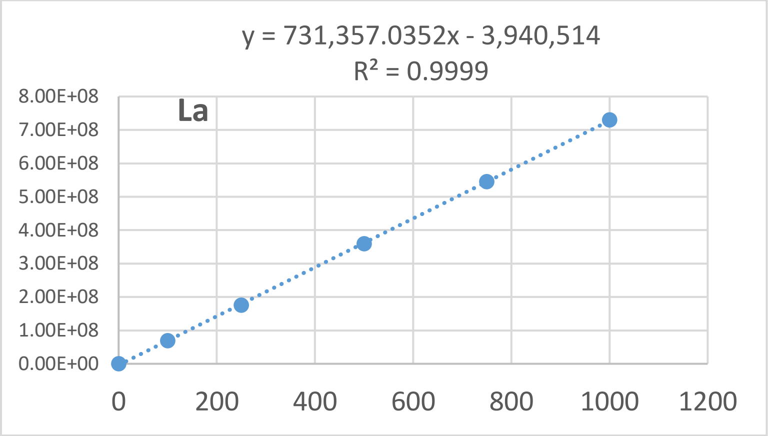

Figure S32. ICP calibration curve for lanthanum. Values on the abscissa axis represent mass fraction in ppb.

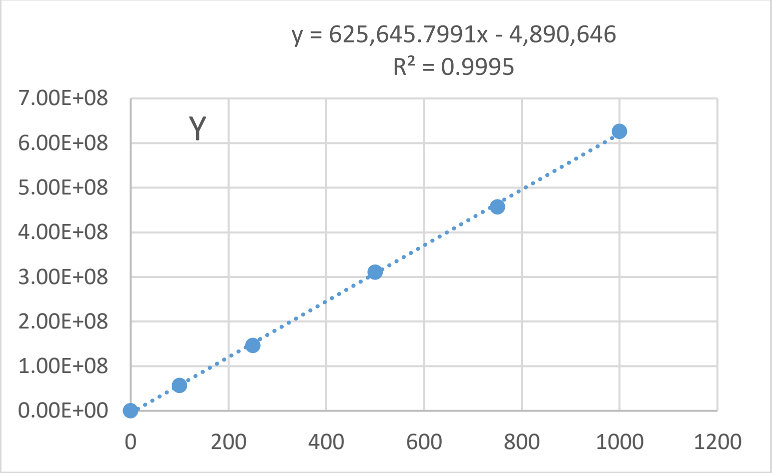

Figure S33. ICP calibration curve for yttrium. Values on the abscissa axis represent mass fraction in ppb.

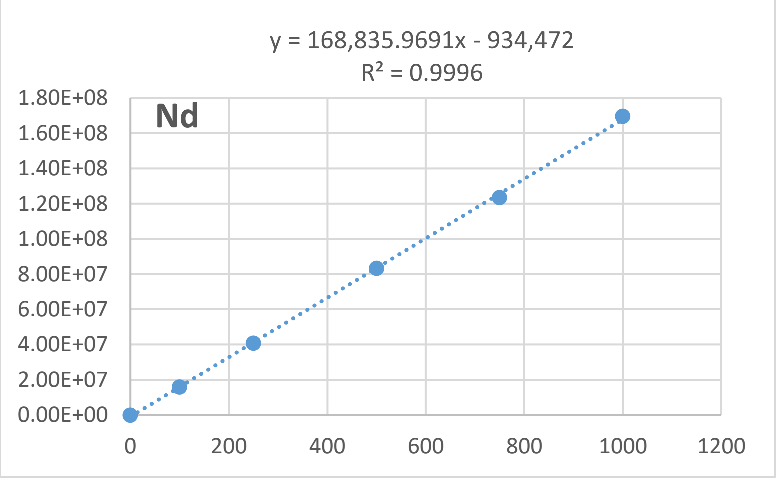

Figure S34. ICP calibration curve for neodymium. Values on the abscissa axis represent mass fraction in ppb.

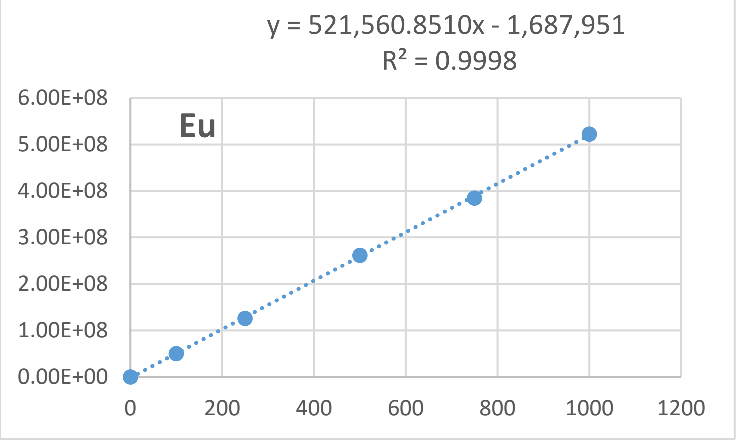

Figure S35. ICP calibration curve for europium. Values on the abscissa axis represent mass fraction in ppb.

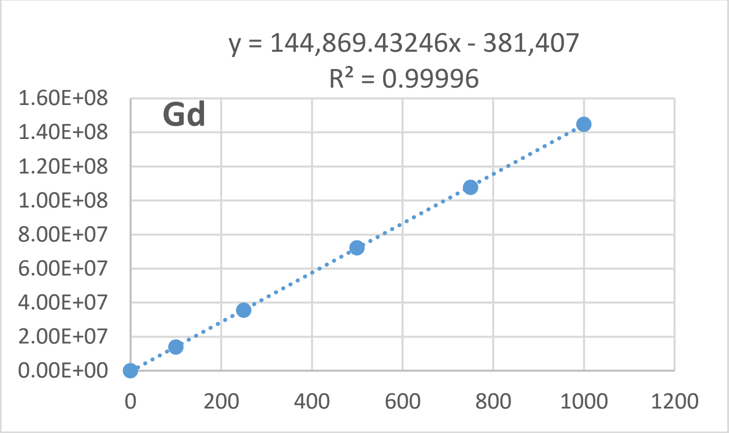

Figure S36. ICP calibration curve for gadolinium. Values on the abscissa axis represent mass fraction in ppb.

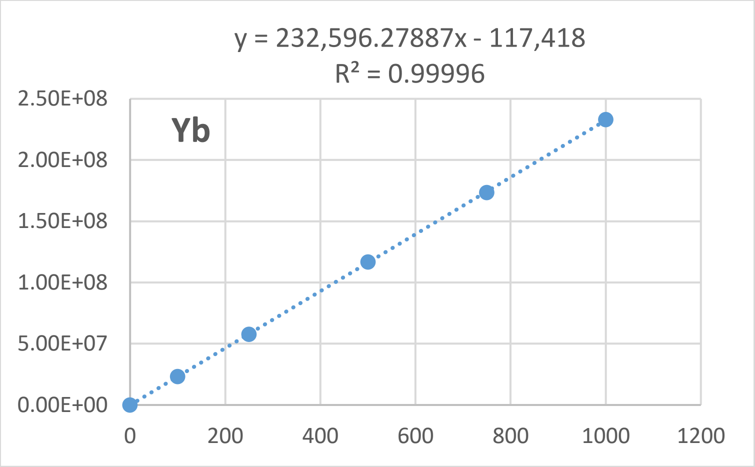

Figure S37. ICP calibration curve for ytterbium. Values on the abscissa axis represent mass fraction in ppb.

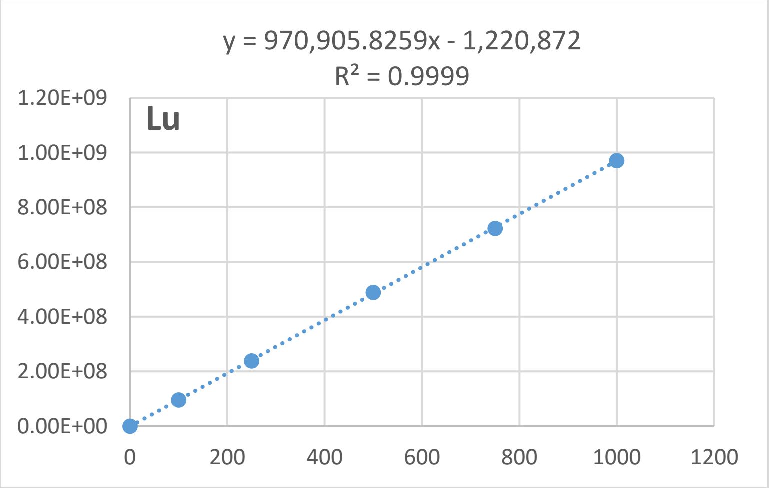

Figure S38. ICP calibration curve for scandium. Values on the abscissa axis represent mass fraction in ppb.

5.2. Separation Results

Table S1. Results of separation of Sc from a mixture of rare earth oxides using sodium oxalate. The n_{aq} fraction represents metals in solution, while n_r fraction represents metals in solid residue. Δn represents associated errors for both values.

	n_{aq} / mmol	**Δn_{aq} / mmol**	**n_r / mmol**	**Δnr / mmol**
Sc	2.423267	0.014273	0.068546	0.000609
Y	0.225129	0.003928	2.271414	0.038846
La	0.158318	0.002477	1.914352	0.005017
Nd	0.081632	0.000649	1.89204	0.022194
Eu	0.06695	0.001143	2.163308	0.011957
Gd	0.065228	0.000652	2.201607	0.029685
Yb	0.405507	0.005421	1.787233	0.015779
Lu	0.645144	0.010021	1.581554	0.016417

Table S2. Results of separation of Sc from a mixture of rare earth oxides using ammonium oxalate. The n_{aq} fraction represents metals in solution, while n_r fraction represents metals in solid residue. Δn represents associated errors for both values.

	n_{aq} / mmol	**Δn_{aq} / mmol**	**n_r / mmol**	**Δn_r / mmol**
Sc	2.449203	0.028363	0.137791	0.001647
Y	0.187409	0.001307	2.305207	0.029294
La	0.024806	0.000474	2.136389	0.046474
Nd	0.016085	0.000258	1.96367	0.051862
Eu	0.031164	0.000323	2.258656	0.020511
Gd	0.039839	0.000665	2.403468	0.043294
Yb	0.367798	0.003611	1.866504	0.018584
Lu	0.46188	0.004618	1.840021	0.006702

6. Thermogravimetric Analysis / Differential Scanning Calorimetry

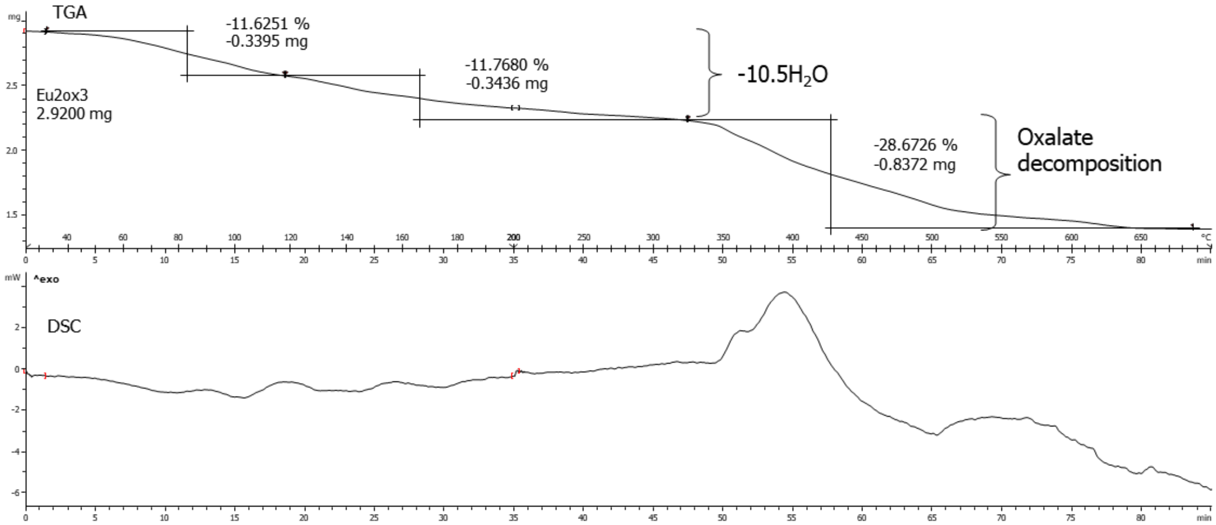

Figure S39. TGA/DSC curve for the decomposition of Eu_2**ox**$_3$ · 10.5H_2O. Measurements were performed in nitrogen until 200 °C and in air from 200 °C to 700 °C to ensure oxalate decomposition.

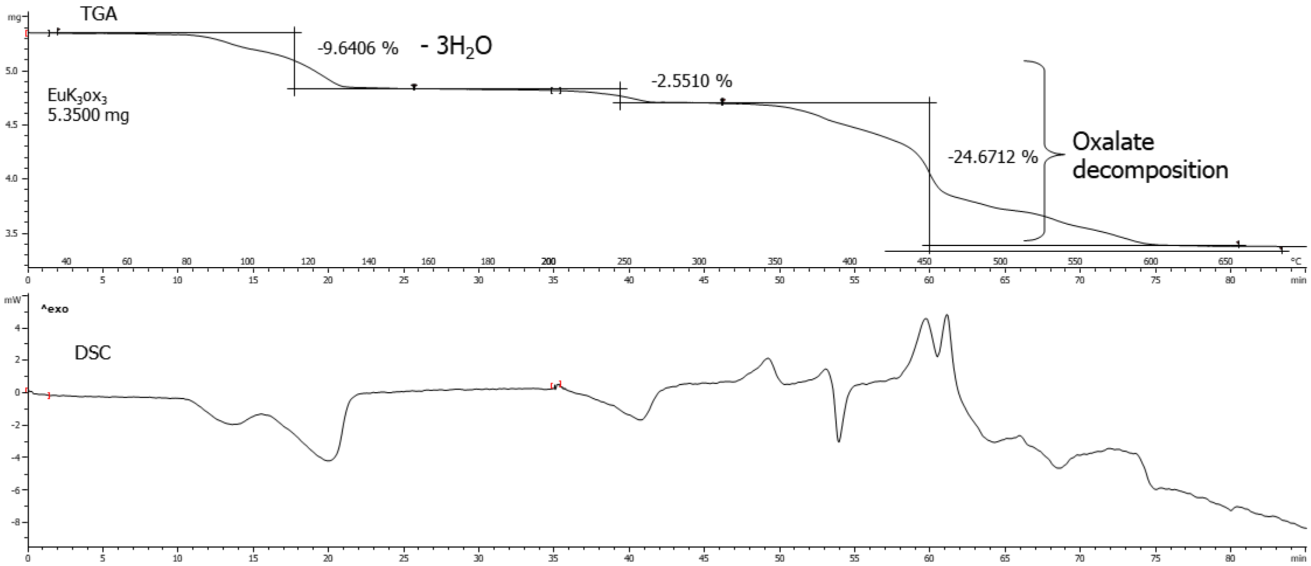

Figure S40. TGA/DSC curve for the decomposition of K_3Eu**ox**$_3$ · 3H_2O. Measurements were performed in nitrogen until 200 °C and in air from 200 °C to 700 °C to ensure oxalate decomposition.

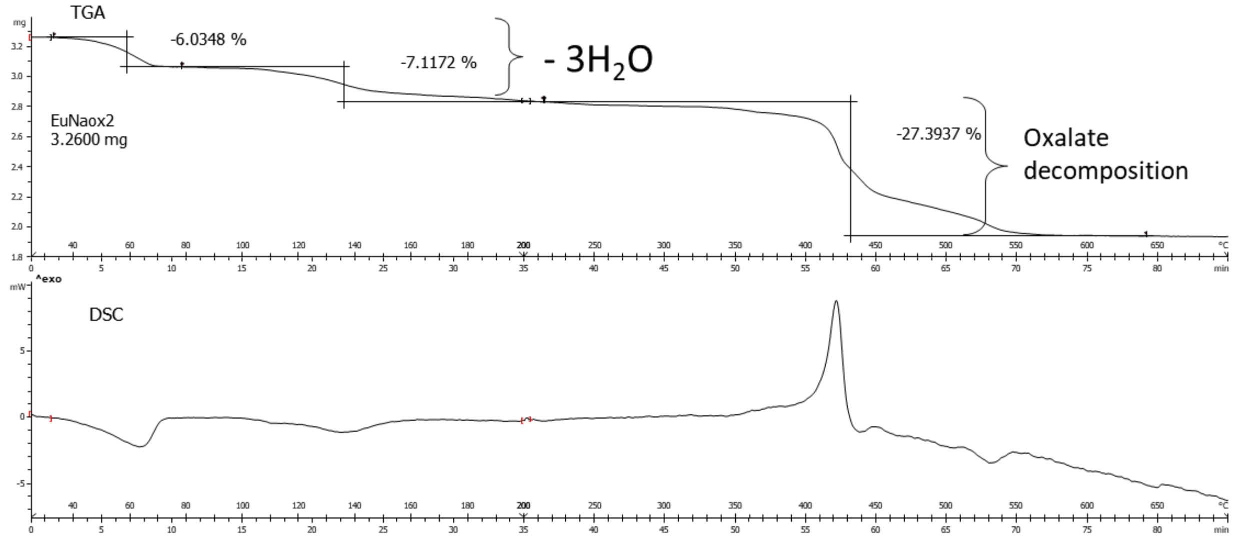

Figure S41. TGA/DSC curve for the decomposition of NaEu**ox**$_2$ · 3H_2O. Measurements were performed in nitrogen until 200 °C and in air from 200 °C to 700 °C to ensure oxalate decomposition. Crystal structure analysis indicates that the formula unit should contain 4 water molecules, however the mass loss corresponds to only 3 water molecules.

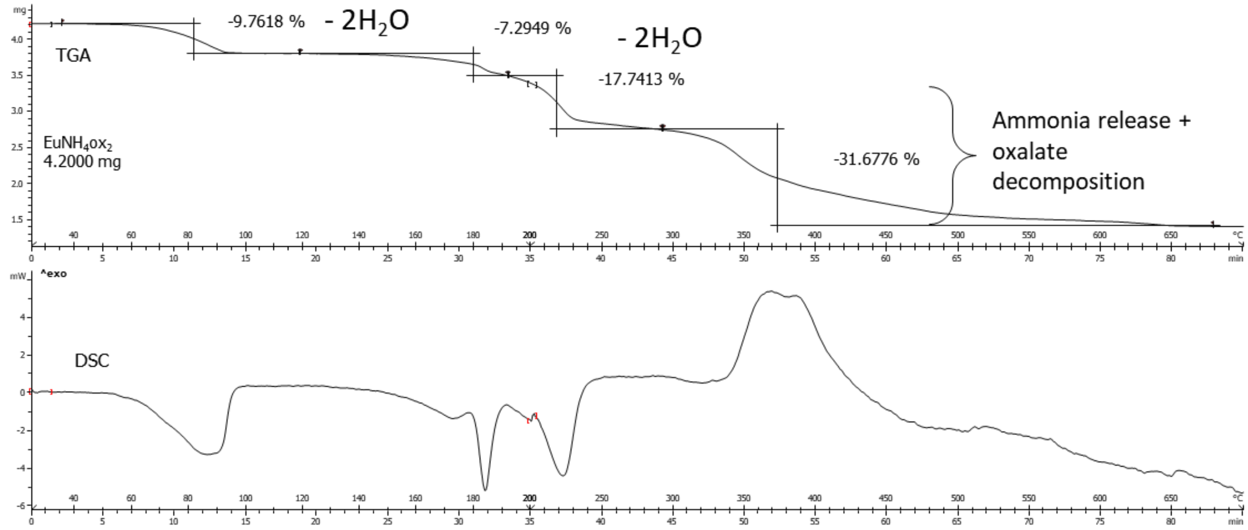

Figure S42. TGA/DSC curve for the decomposition of (NH_4)Eu**ox**$_2$ · 4H_2O. Measurements were performed in nitrogen until 200 °C and in air from 200 °C to 700 °C to ensure oxalate decomposition.

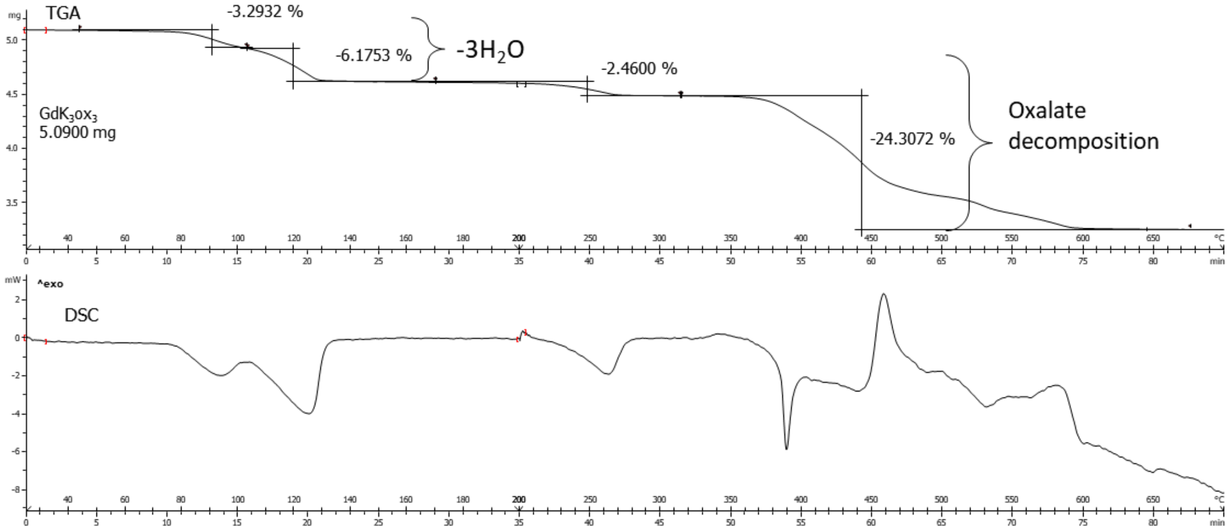

Figure S43. TGA/DSC curve for the decomposition of $K_3Gd\mathbf{ox}_3 \cdot 3H_2O$. Measurements were performed in nitrogen until 200 °C and in air from 200 °C to 700 °C to ensure oxalate decomposition.

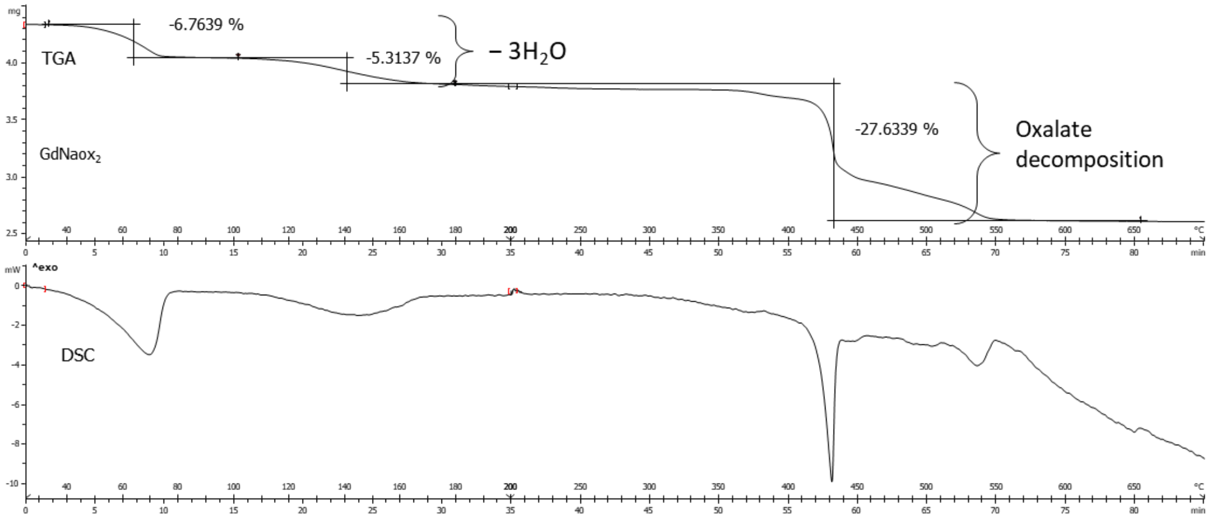

Figure S44. TGA/DSC curve for the decomposition of $NaGd\mathbf{ox}_2 \cdot 4H_2O$. Measurements were performed in nitrogen until 200 °C and in air from 200 °C to 700 °C to ensure oxalate decomposition. Crystal structure analysis indicates that the formula unit should contain 4 water molecules, however the mass loss corresponds to only 3 water molecules.

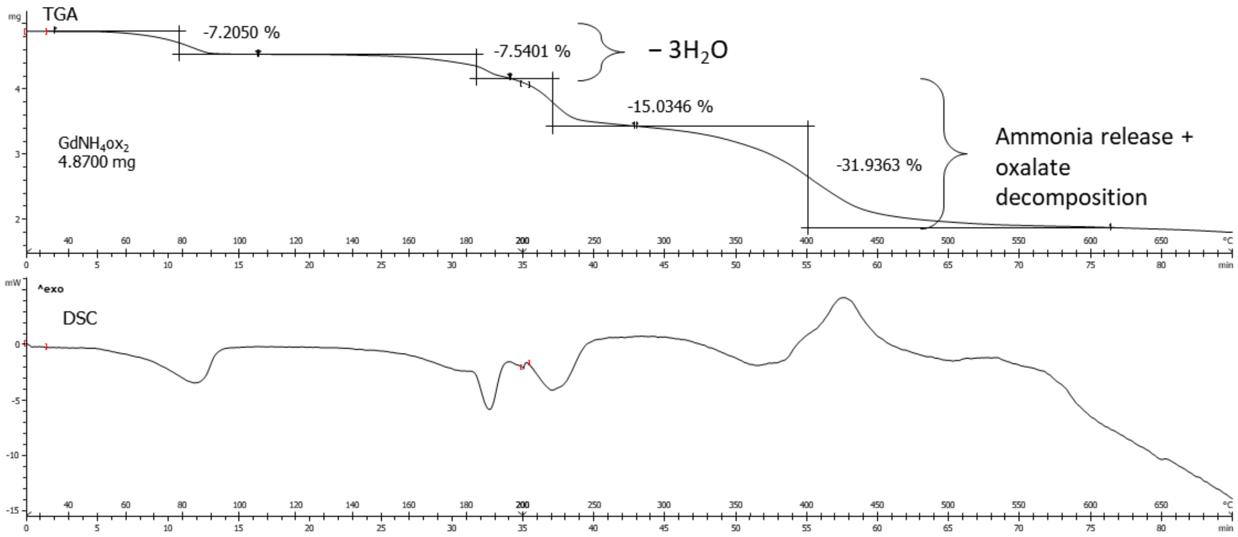

Figure S45. TGA/DSC curve for the decomposition of $(NH_4)Gd\mathbf{ox}_2 \cdot 3H_2O$. Measurements were performed in nitrogen until 200 °C and in air from 200 °C to 700 °C to ensure oxalate decomposition.

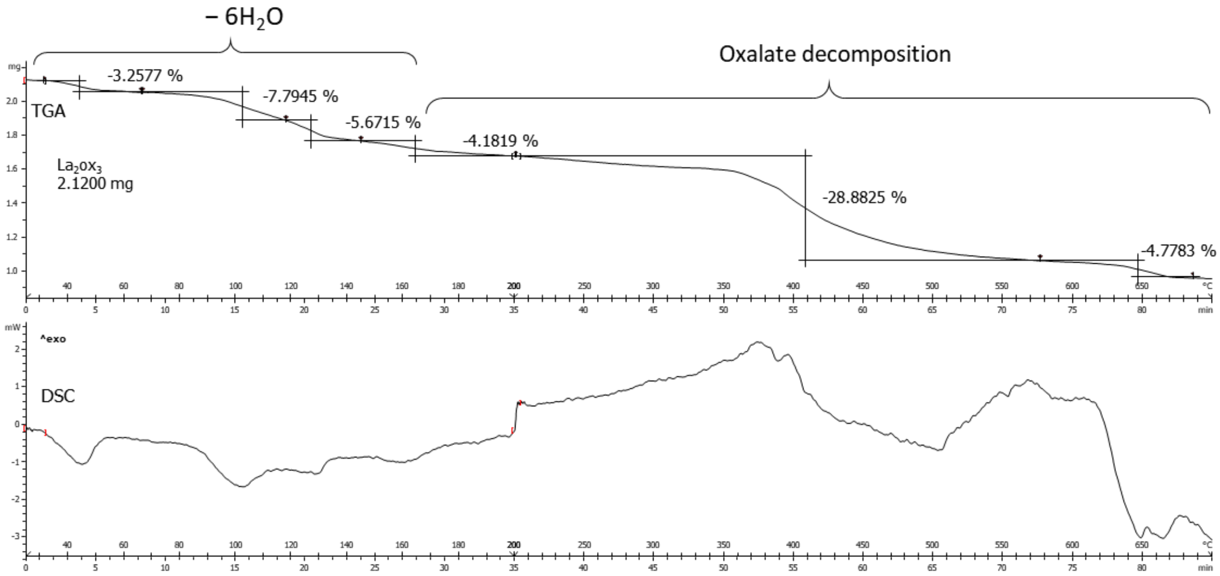

Figure S46. TGA/DSC curve for the decomposition of $La_2\mathbf{ox}_3 \cdot 6H_2O$. Measurements were performed in nitrogen until 200 °C and in air from 200 °C to 700 °C to ensure oxalate decomposition.

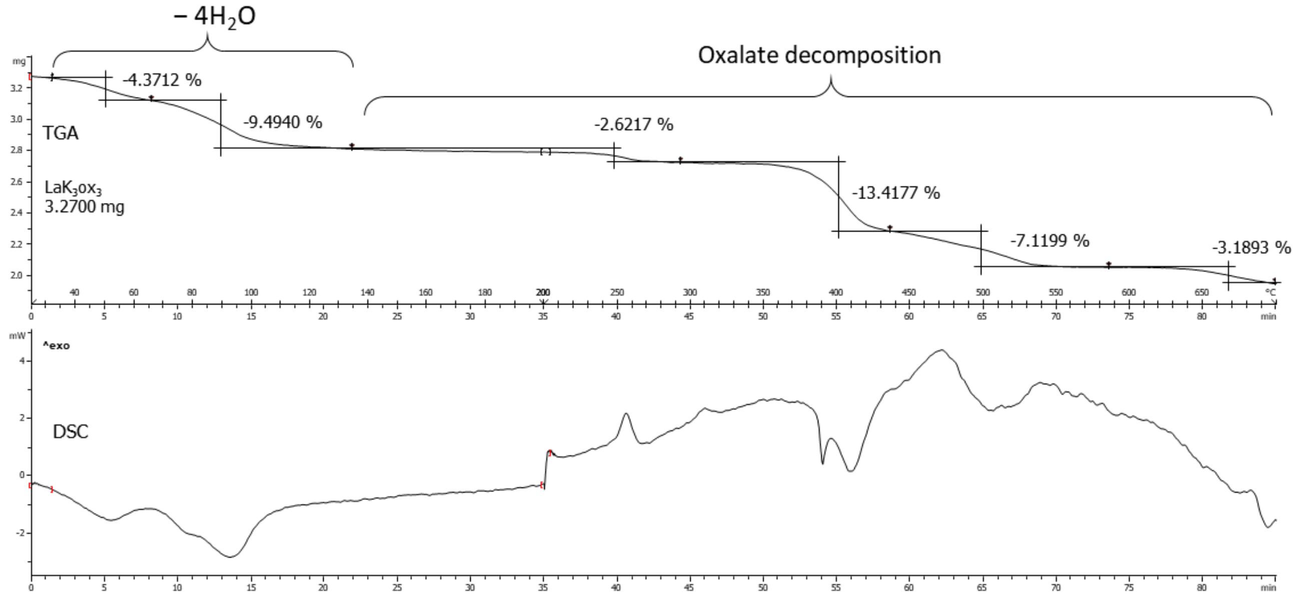

Figure S47. TGA/DSC curve for the decomposition of K$_3$La**ox**$_3$ · 4H$_2$O. Measurements were performed in nitrogen until 200 °C and in air from 200 °C to 700 °C to ensure oxalate decomposition.

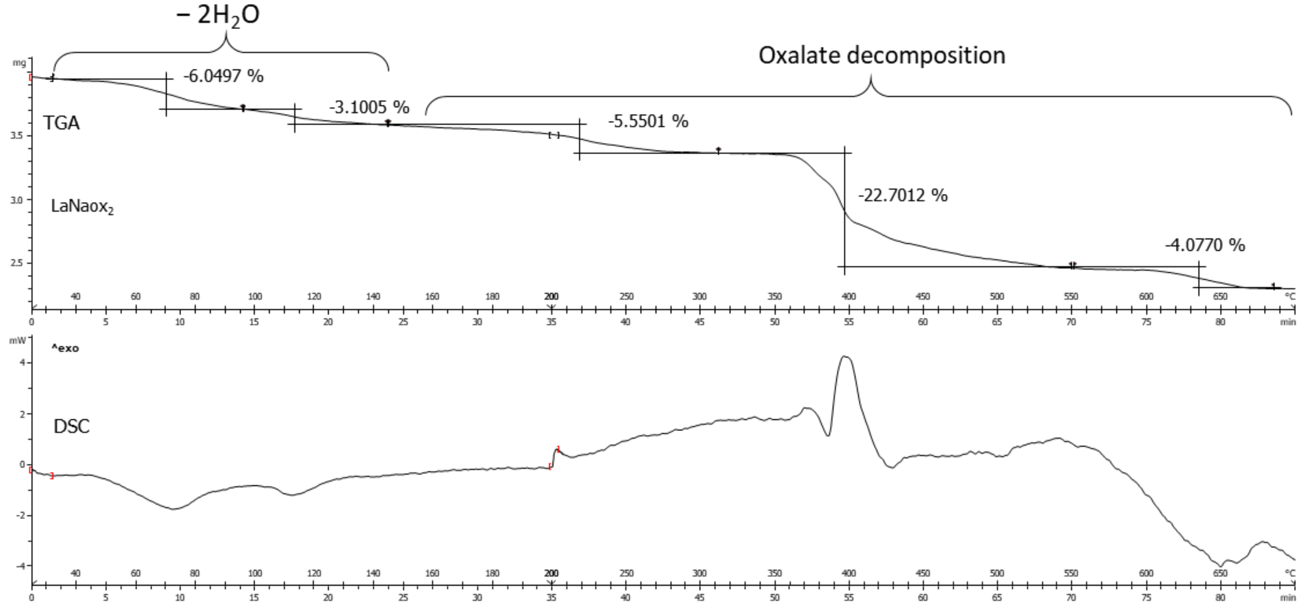

Figure S48. TGA/DSC curve for the decomposition of NaLa**ox**$_2$ · 2H$_2$O. Measurements were performed in nitrogen until 200 °C and in air from 200 °C to 700 °C to ensure oxalate decomposition.

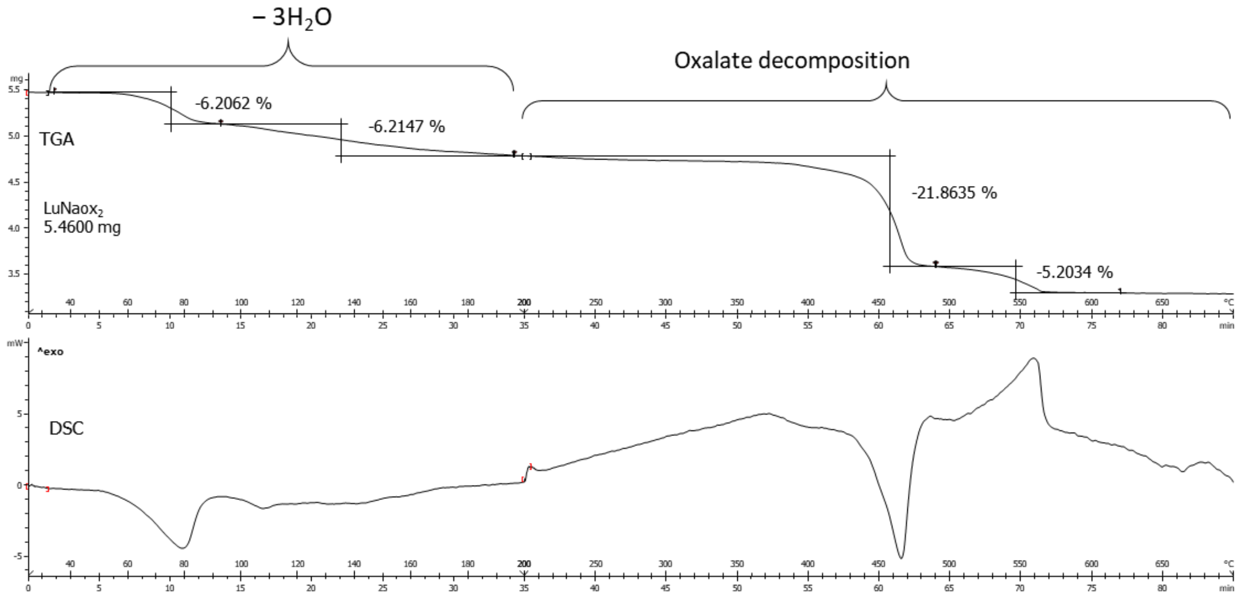

Figure S49. TGA/DSC curve for the decomposition of NaLu**ox**$_2$ · $4H_2O$. Measurements were performed in nitrogen until 200 °C and in air from 200 °C to 700 °C to ensure oxalate decomposition. Crystal structure analysis indicates that the formula unit should contain 4 water molecules, however the mass loss corresponds to only 3 water molecules.

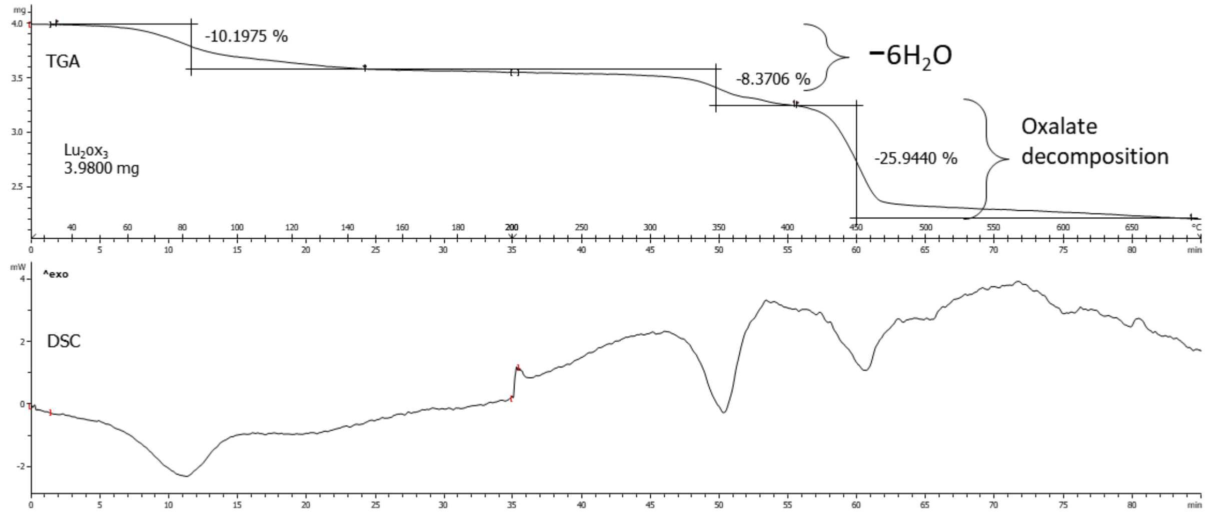

Figure S50. TGA/DSC curve for the decomposition of Lu$_2$**ox**$_3$ · $6H_2O$. Measurements were performed in nitrogen until 200 °C and in air from 200 °C to 700 °C to ensure oxalate decomposition.

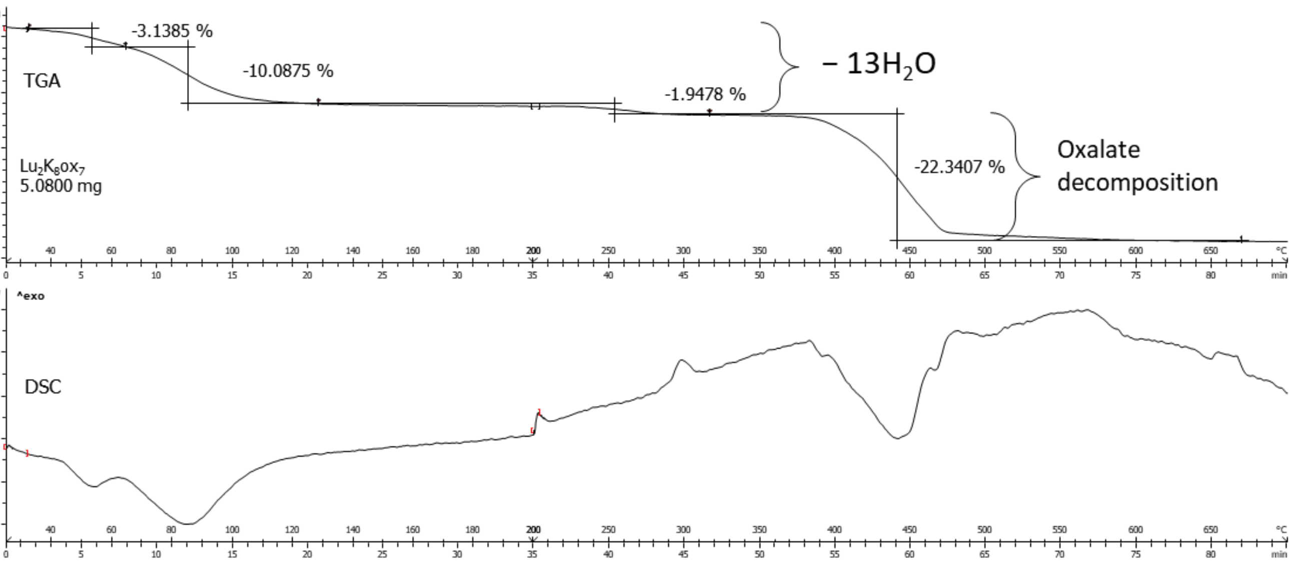

Figure S51. TGA/DSC curve for the decomposition of K_8Lu_2**ox**$_7 \cdot 11H_2O$. Measurements were performed in nitrogen until 200 °C and in air from 200 °C to 700 °C to ensure oxalate decomposition. Crystal structure analysis indicates that the formula unit should contain 14 water molecules, however the mass loss corresponds to only 13 water molecules.

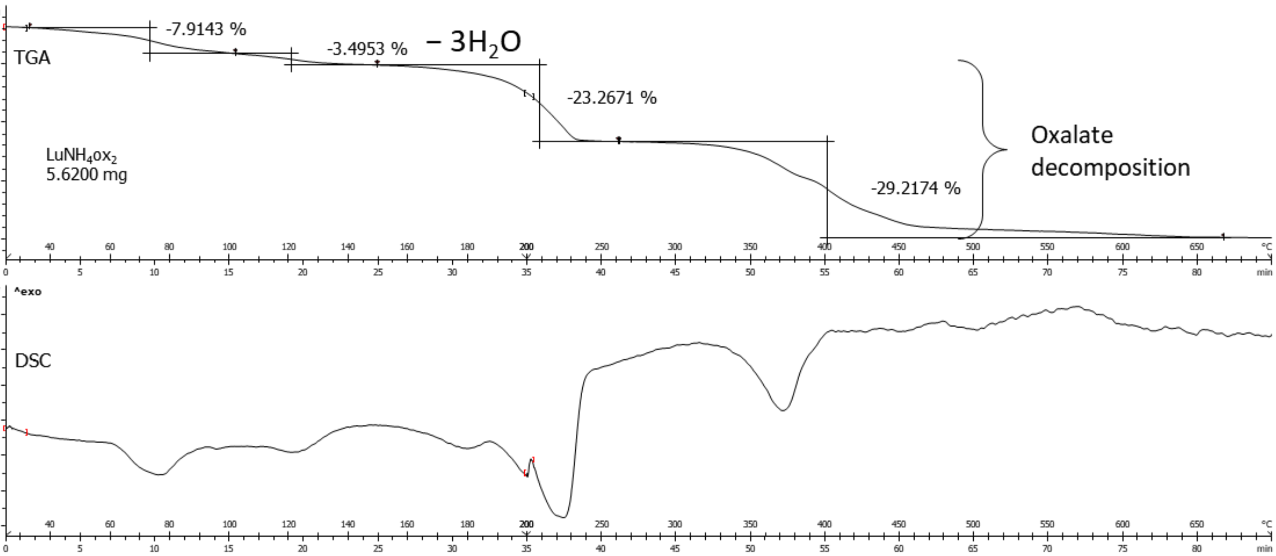

Figure S52. TGA/DSC curve for the decomposition of $(NH_4)Lu$**ox**$_2 \cdot 3H_2O$. Measurements were performed in nitrogen until 200 °C and in air from 200 °C to 700 °C to ensure oxalate decomposition.

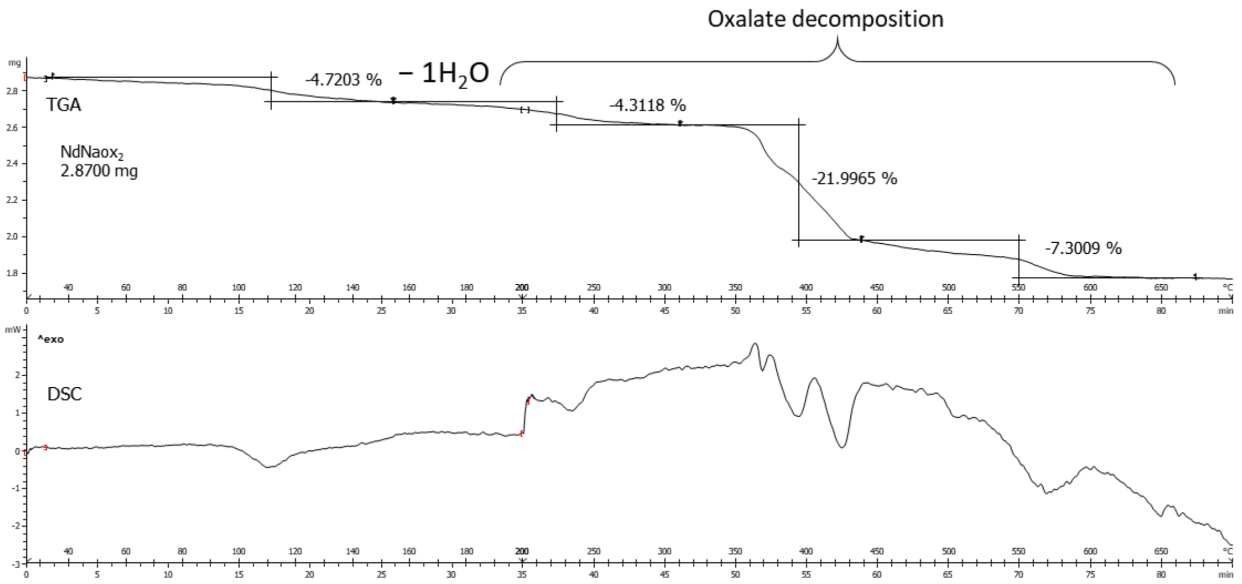

Figure S53. TGA/DSC curve for the decomposition of NaNd**ox**$_2$ · 1H$_2$O. Measurements were performed in nitrogen until 200 °C and in air from 200 °C to 700 °C to ensure oxalate decomposition.

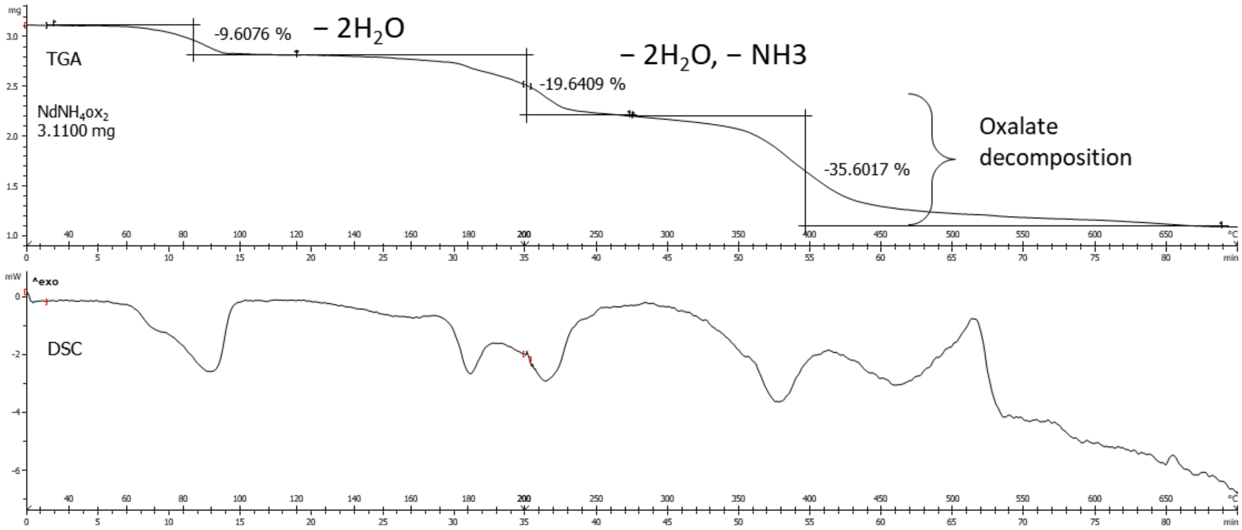

Figure S54. TGA/DSC curve for the decomposition of (NH$_4$)Nd**ox**$_2$ · 4H$_2$O. Measurements were performed in nitrogen until 200 °C and in air from 200 °C to 700 °C to ensure oxalate decomposition.

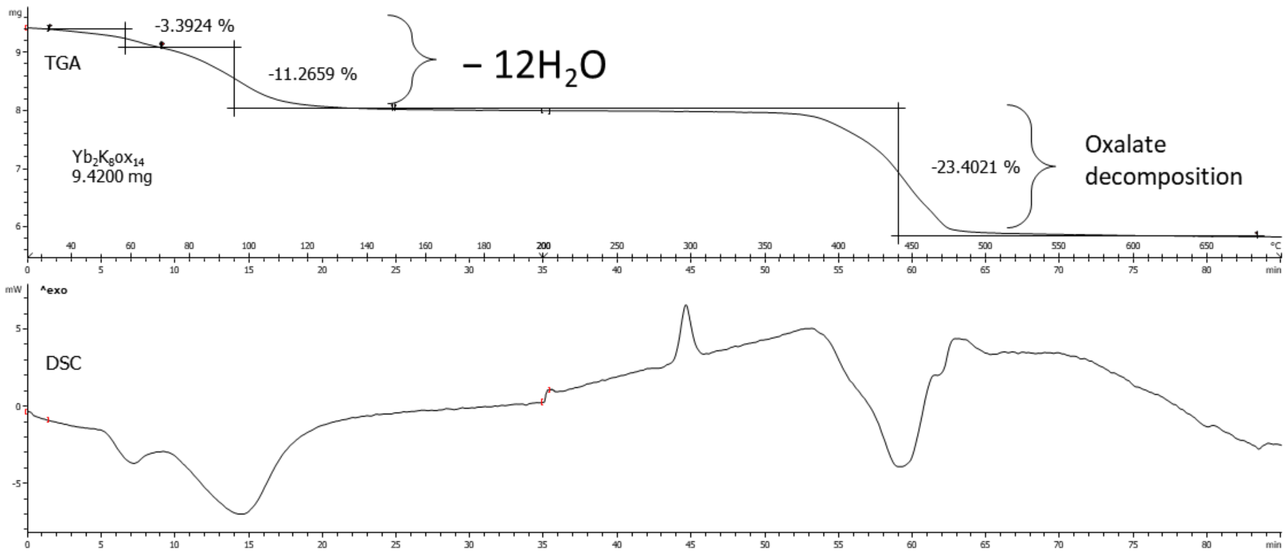

Figure S55. TGA/DSC curve for the decomposition of K_8Yb_2**ox**$_7 \cdot 14H_2O$. Measurements were performed in nitrogen until 200 °C and in air from 200 °C to 700 °C to ensure oxalate decomposition. Crystal structure analysis indicates that the formula unit should contain 14 water molecules, however the mass loss corresponds to only 12 water molecules.

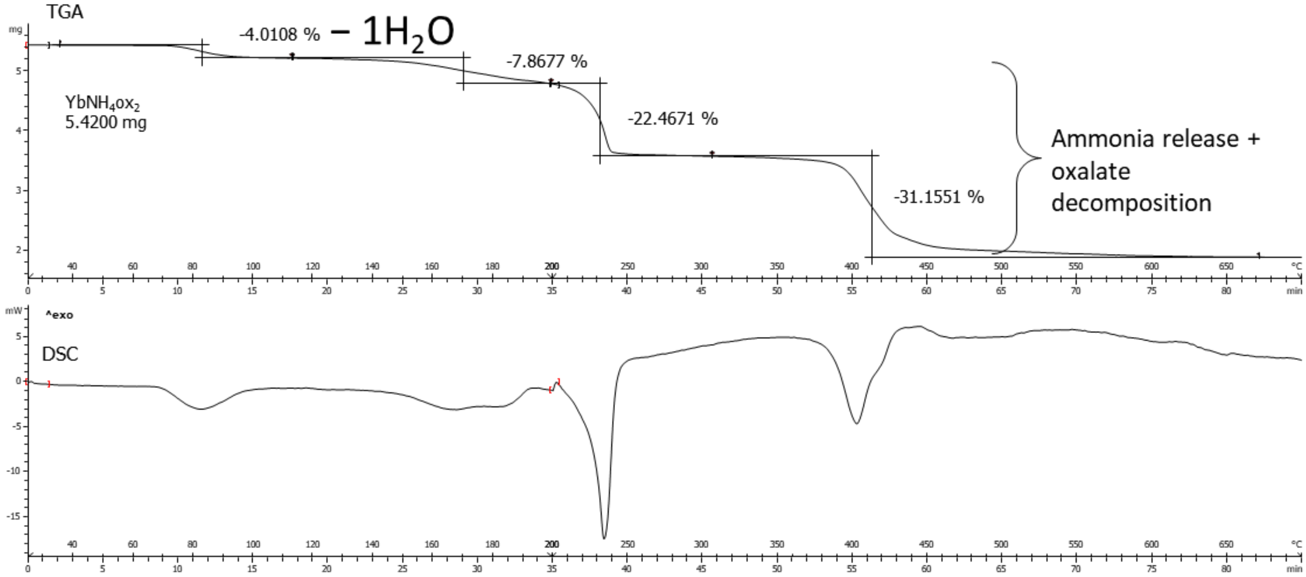

Figure S56. TGA/DSC curve for the decomposition of $(NH_4)Yb$**ox**$_2 \cdot 1H_2O$. Measurements were performed in nitrogen until 200 °C and in air from 200 °C to 700 °C to ensure oxalate decomposition.

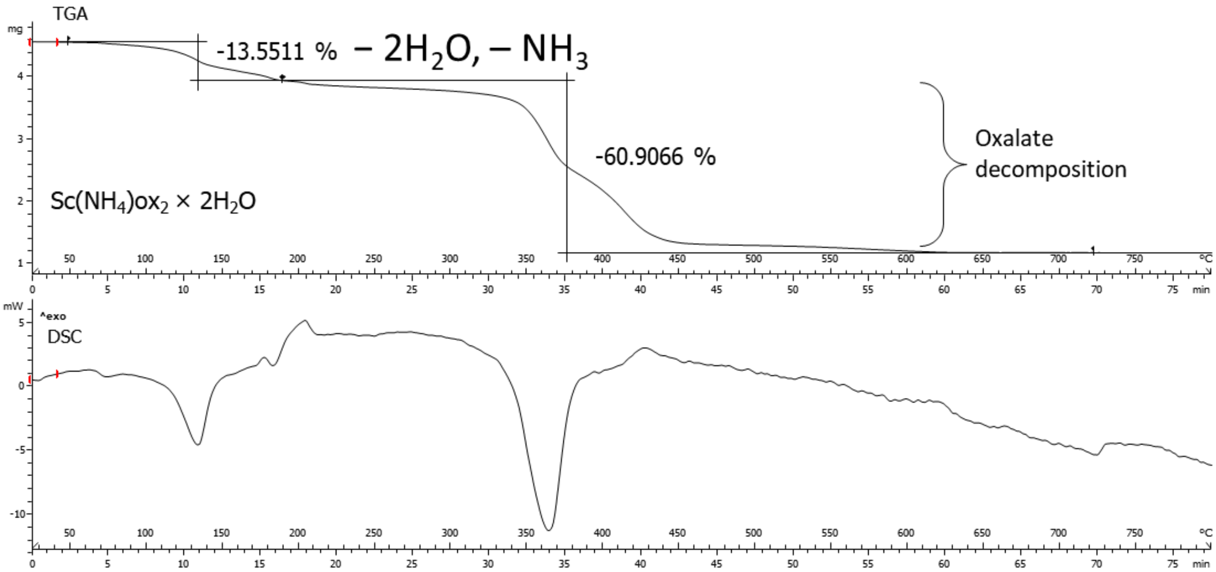

Figure S57. TGA/DSC curve for the decomposition of $(NH_4)Sc\mathbf{ox}_2 \cdot 2H_2O$.

7. Infrared spectra

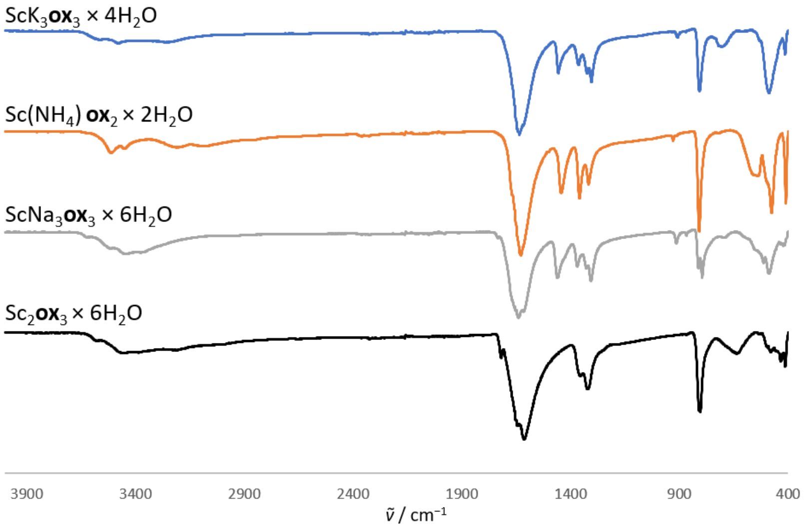

Figure S58. IR ATR spectra of scandium oxalates prepared in this work.

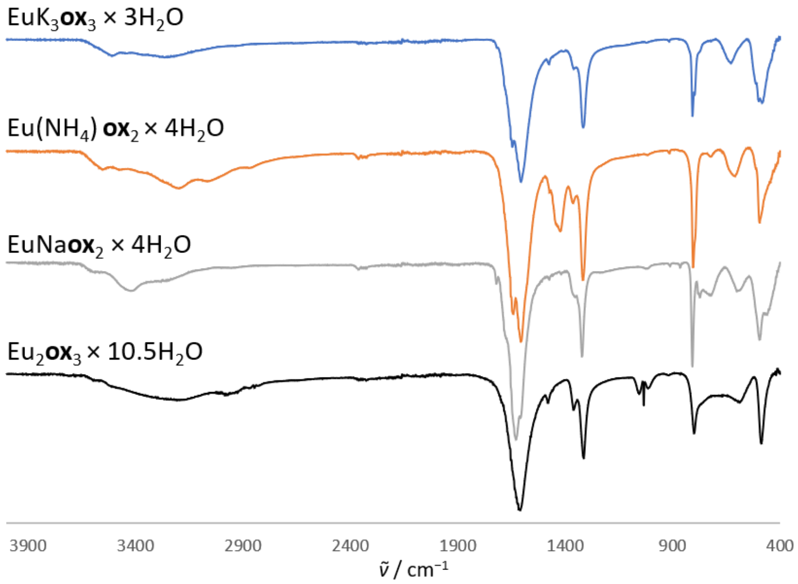

Figure S59. IR ATR spectra of europium oxalates prepared in this work.

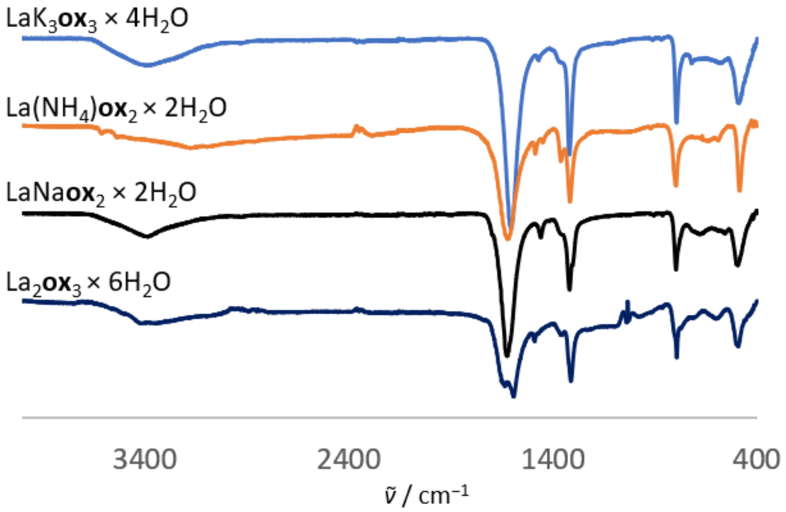

Figure S60, IR ATR spectra of lanthanum oxalates prepared in this work.

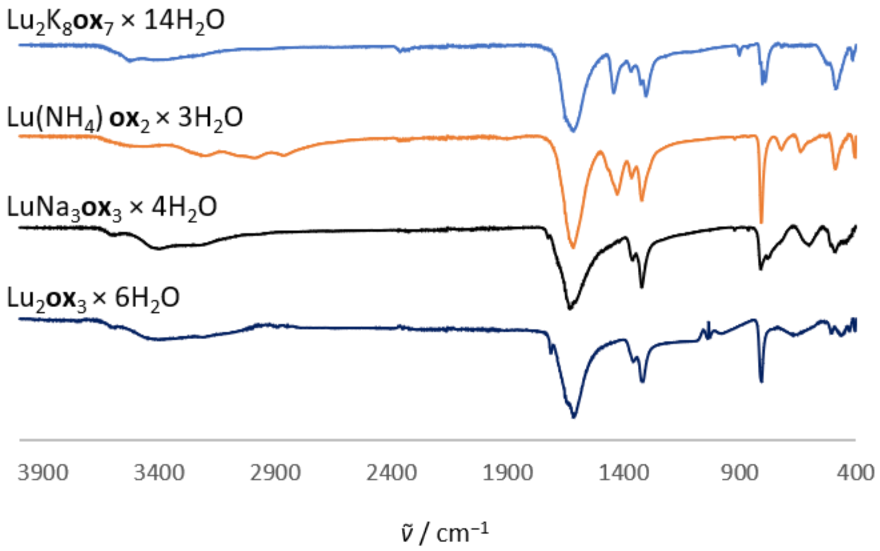

Figure S61. IR ATR spectra of lutetium oxalates prepared in this work.

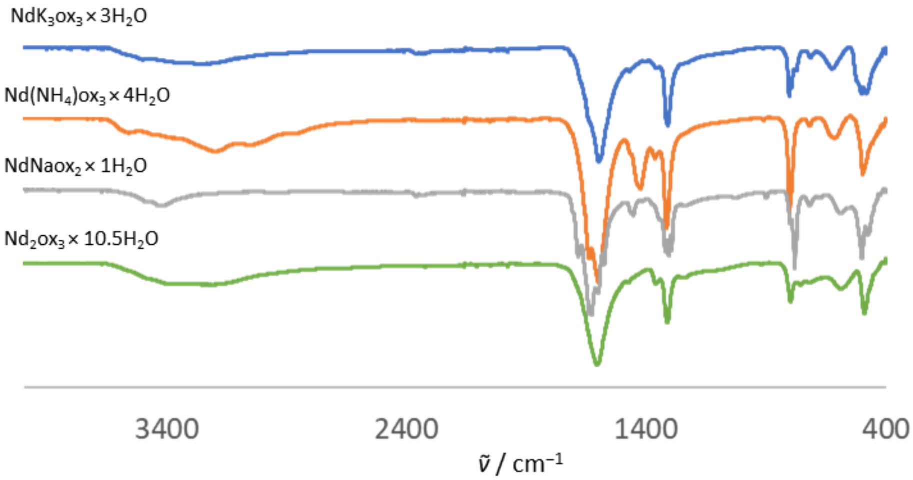

Figure S62. IR ATR spectra of neodymium oxalates prepared in this work.

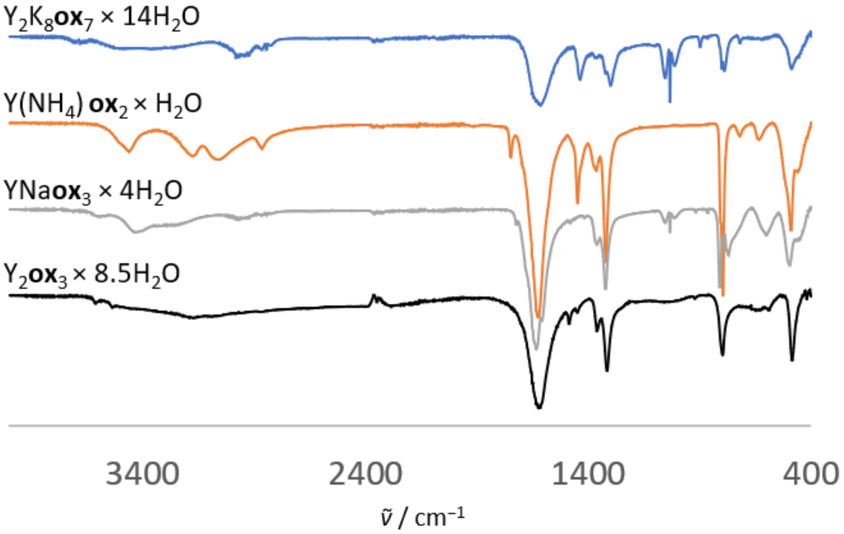

Figure S63. IR ATR spectra of yttrium oxalates prepared in this work.

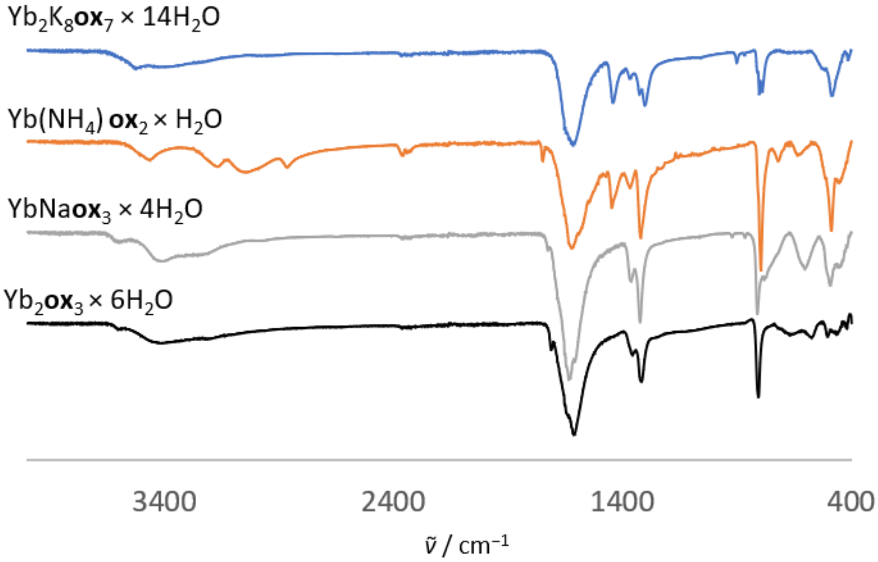

Figure S64. IR ATR spectra of ytterbium oxalates prepared in this work.

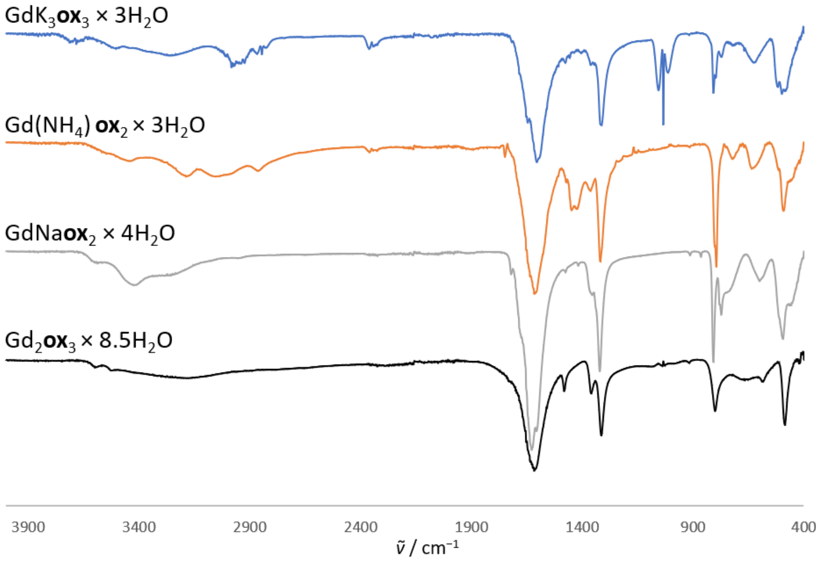

Figure S65. IR ATR spectra of gadolinium oxalates prepared in this work.

8. Geometrical Analysis

Table S3. Coordination numbers (CN) and corresponding coordination polyhedra of the RE^{3+} metal nodes in the investigated structures. Phases are designated by the CSD code of the structure of the corresponding metal oxalates, or the CSD code for a metal oxalate structure that appears isostructural to the reaction product. Shaded cells highlight novel phases that structurally resemble those corresponding to the given CSD code; the coordination environment of these phases has been estimated based on the similarity between known phases.

RE	Oxalic acid	CN	Coord. polyhedron	NH$_4$	CN	Coord. polyhedron	Na	CN	Coord. polyhedron	K	CN	Coord. polyhedron
Sc	AOXSCH	8	square antiprism	**2**	8	square antiprism	**4**	8	square antiprism	**5**/**6** mixture	8[a]	square antiprism[a]
Y	VEXPUK / YOXALT	9[a]	capped square antiprism[a]	AYOXLH	9	capped square antiprism	BOMLEU	9	capped square antiprism	CIBZAO	8	square antiprism
Yb	AOXYBH	8	square antiprism	**3**	9	capped square antiprism	SEYKOX	9	capped square antiprism	CIBZAO	8	square antiprism
Lu	AOXYBH	8	square antiprism	Unknown	?	Unknown	BOMLEU	9	capped square antiprism	CIBZAO	8	square antiprism
La	Unknown	?	Unknown	QUHYIB	10	bicapped square antiprism	Unknown	?	Unknown	Unknown	?	Unknown
Nd	NDOXAL	9	capped square antiprism	YEBKOG	9	capped square antiprism	Unknown	?	Unknown	DEXXOU/**7**	9[a]	capped square antiprism[a]
Eu	NDOXAL	9	capped square antiprism	YEBKOG	9	capped square antiprism	BOMLEU	9	capped square antiprism	DEXXOU/**7**	9[a]	capped square antiprism[a]
Gd	VEXPUK / YOXALT	9[a]	capped square antiprism[a]	YEBKOG	9	capped square antiprism	BOMLEU	9	capped square antiprism	DEXXOU/**7**	9[a]	capped square antiprism[a]

[a] coordination descriptors for both phases in the mixture are the same.

9. References

1 L. Greenspan, *J. Res. Natl. Bur. Stand. Sect. A Phys. Chem.*, 1977, **81A**, 89.

2 N. Kourkoumelis, *Powder Diffr.*, 2013, **28**, 137–148.

3 G. M. Sheldrick, *Acta Crystallogr. Sect. A Found. Crystallogr.*, 2015, **71**, 3–8.

4 G. M. Sheldrick, *Acta Crystallogr. Sect. C Struct. Chem.*, 2015, **71**, 3–8.

5 A. Boultif and D. Louer, *J. Appl. Cryst.*, 2004, **37**, 724–731.

6 W. I. F. David, K. Shankland, J. van de Streek, E. Pidcock, W. D. S. Motherwell and J. C. Cole, *J. Appl. Cryst.*, 2006, **39**, 910–915.

7 G. S. Pawley, *J. Appl. Cryst.*, 1981, **14**, 357–361.

8 A. Coelho, TOPAS Academic 6, Coelho Software, 2016, Brisbane Australia

9 H. M. Rietveld, *J. Appl. Cryst.*, 1969, **2**, 65–71.